

Article

Photocatalytic Degradation of Diazo Dye over Suspended and Immobilized TiO₂ Catalyst in Swirl Flow Reactor: Kinetic Modeling

Waleed Jadaa, Anand Prakash and Ajay K. Ray * 

Department of Chemical and Biochemical Engineering, The University of Western Ontario, London, ON N6A 5B9, Canada; wjadaa@uwo.ca (W.J.); aprakas2@uwo.ca (A.P.)

* Correspondence: aray@eng.uwo.ca

Abstract: The degradation kinetics of Direct Blue 15 (DB15), a diazo dye, were studied over a suspended and immobilized TiO₂ catalyst. For all experiments, the kinetics experiments were performed in a swirl flow photoreactor under the influence of UV light. The effect of different parameters: dye concentration, catalyst loading, and light intensity, on the DB15 kinetics was investigated. The kinetic rates were assessed using apparent (k_a) approach, a single value of reaction rate (k_r) and adsorption constant (K), and approach of k_r as of variable. The DB15 mineralization was discussed as well. Using a dip-coating device, the P25 catalyst was deposited on a Pyrex glass. The thin film surface characterization was examined. The coated catalyst was evaluated by checking the effect of two variables: initial dye concentration and light intensity on the DB15 kinetics. In terms of the k_a approach, the results demonstrated that DB15 degradation is described by the pseudo first-order kinetics model. The Langmuir-Hinshelwood (L-H) model was fitted well with the experimental data for the number of process variables. L-H constant k_r was determined as a function of three parameters: initial dye concentration, catalyst loading, and light intensity. The k_a values were evaluated and compared with experimental results. In terms of three variables, k_a can be expressed as $k_a = \frac{0.15 [C]_o^{-0.69} [W]^{0.73} I^{0.91}}{1+0.17 [C]_o}$ while the empirical model results in the following expression, $k_a = 0.77 [C]_o^{-1.65} [W]^{0.73} I^{0.89}$. It was observed that 83.64% mineralization was achieved after a period of 16 hrs. In terms of immobilized catalyst, the DB15 degradation kinetics was described by a pseudo first-order model for different dye concentrations. Meanwhile, a power-law model described the impact of light intensity on dye kinetics. In addition, the coated catalyst was successfully reusable with high efficiency for up to four cycles.

Keywords: photocatalysis; diazo dye; direct blue 15; swirl-flow reactor; degradation; kinetics; Langmuir-Hinshelwood model



Citation: Jadaa, W.; Prakash, A.; Ray, A.K. Photocatalytic Degradation of Diazo Dye over Suspended and Immobilized TiO₂ Catalyst in Swirl Flow Reactor: Kinetic Modeling. *Processes* **2021**, *9*, 1741. <https://doi.org/10.3390/pr9101741>

Academic Editors: Maria Jose Martin de Vidales, Sara Mateo Fernandez and José Fernando Pérez

Received: 30 August 2021

Accepted: 20 September 2021

Published: 28 September 2021

Publisher's Note: MDPI stays neutral with regard to jurisdictional claims in published maps and institutional affiliations.



Copyright: © 2021 by the authors. Licensee MDPI, Basel, Switzerland. This article is an open access article distributed under the terms and conditions of the Creative Commons Attribution (CC BY) license (<https://creativecommons.org/licenses/by/4.0/>).

1. Introduction

Water pollution is continuously gaining great interest globally due to its health implications. Within the last few decades, tremendous efforts have been invested into water and/or wastewater treatment applications to reduce environmental problems and achieve protection for humans and the environment [1,2]. The presence of organic pollutants such as colored dyes in industrial aqueous effluents is considered a major environmental issue. If the colored wastewater reaches the surface and/or ground water, it can result in contamination of the drinking water system. This is a serious problem that threatens human health [3,4]. Additionally, the degradation of these dyes yields undesirable by-products [5]. More precisely, most dyes and their by-products are carcinogenic and toxic compounds [6–8]. Furthermore, the presence of such colored dyes in effluents can directly harm aquatic species. Due to water reflection, colored dyes can reduce water transparency. Hence, the level of sunlight penetrating the water is decreased, resulting in a negative

impact on the photosynthetic process, which eventually affects aquatic systems [9,10]. Therefore, it is not a surprise that wastewater that contains dye is considered one of the major sources of water pollution [5].

Over the years, several processes have been proposed to destroy these pollutants [3,4,10–16]. In recent years, processes based on photocatalytic degradation of the toxins have been getting more attention since complete mineralization of the organic pollutant can be achieved in the presence of catalyst particles [12–17]. The catalyst particles are oxides of semiconducting materials, among which TiO₂ has been used mostly due to low cost, non-toxicity, and high stability [17–21].

It has been widely found that the degradation rate of different dyes via heterogeneous photocatalytic oxidation follows the Langmuir-Hinshelwood (L-H) kinetics model [11–19]. This model provides the following relationship between the degradation rate and the substrate concentration.

$$r_i = -\frac{dC_i}{dt} = k_{ri} \frac{K_i \cdot C_i}{1 + \sum_i K_i \cdot C_i} \quad (1)$$

where k_{ri} is the reaction rate constant ($\text{mg L}^{-1} \text{min}^{-1}$), and K_i is the adsorption coefficient for the substrate on the photocatalyst surface.

Literature studies have used simplifications to the above model to drive applicable kinetic parameters for the conditions investigated [13,15,17,20–24]. A commonly used expression is obtained from Equation (1) for a single component system and dilutes concentrations (i.e., $K_i C_i \ll 1$):

$$r = -\frac{dC}{dt} = k_r K \cdot C = k_a C \quad (2)$$

where k_a refers to the pseudo first-order rate constant or apparent rate constant.

It may be noted that kinetic parameters in Equations (1) and (2) do not account for the impact of different factors such as light intensity and initial dye concentration on k_r and K , which limits their applicability to a range of specified operating conditions. Based on their study, Turchi and Ollis [25] proposed a model that assumes that K is independent of light intensity. They explained that it is related to the adsorptive affinity of an organic substrate on the catalyst surface. Hence, it is considered as a characteristic property that cannot be changed for that organic substrate, though it could completely differ from other substrate types. In contrast, Xu and Langford [19] observed an opposite behavior. During experiments of photodegradation of acetophenone over TiO₂ Degussa P25, it was noticed that K is related to light intensity. This behaviour was attributed to a change in the electronic properties of catalyst surface due to irradiation that possibly leads to a change and/or improvement in the catalyst's adsorption sites. In their study, the researchers found that k_r increases as the light intensity is increased. Similarly, Meng et al. [18] found that both k_r and K are light intensity-dependant. Their study found that the mentioned constants are linearly proportional to the intensity's square root for the photocatalytic degradation of para-chlorobenzoate over TiO₂ Degussa P25. By fitting the proposed models to the experimental data, the validity of such models was relatively proven. Zhou and Ray [26] stated that the k_r of a photodegradation reaction is typically correlated with light intensity as a power-law relationship. However, it was previously found that the value of k_r is related to the square root of the light intensity for high-intensity ranges, whereas its value is linearly proportional to the light intensity at low-intensity ranges. In their study, the photodegradation of Eosin over immobilized Degussa P25 TiO₂ was investigated. The k_r values were evaluated as a function of two parameters: light intensity and catalyst loading, instead of a single variable. Behnajady et al. [27] explored the degradation kinetics of Acid Yellow 23 dye using ZnO as photocatalyst. The obtained findings showed that both k_r and K are light intensity dependent. It was found that these constants increase as the light intensity is increased. By inserting the values of k_r and K as a function of light intensity, the Langmuir model was then modified to predict k_a values. The obtained results of the modified model exhibited good agreement with the experimental results.

Hashim et al. [28] concluded that as the light intensity increases, the value of k_r is increased for the photodegradation of Diclofenac over Degussa P25 TiO₂. The correlation was represented by a square root relation in terms of light intensity. Yatmaz et al. [29] observed that the decolorization of Remazol Red (RR) over ZnO is modelled by pseudo first-order reaction kinetics. Their study revealed that the k_a constant is related to catalyst loading and dye concentration as $W^{0.6}$ and $[C]^{-1.5}$, respectively. In addition, the k_a constant was correlated to the square root of the light intensity (I_0). Behnajady & Modirshahla [30] evaluated Acid Red 27 (AR27) degradation using a UV/TiO₂ system. The findings of the study showed that the decolorization of AR27 fits well with pseudo first-order reaction kinetics. Using nonlinear regression, a model was developed for finding k_a in terms of different factors as: $k_a = 0.005W^{0.65}[C]^{-0.96}[O_2]^{0.16}I_0$.

From the catalyst immobilization perspective, Ray & Beenackers [31] deposited TiO₂ (P25) over Pyrex glass to examine the photocatalytic degradation of Special Brilliant Blue (SBB) dye. Their study included two different deposition configurations over & under Pyrex glass using a swirl-flow reactor. True kinetics rates and their constants were evaluated in terms of different variables such as light intensity, angle of light incidence, and amount of catalyst. The influence of mass transfer on the kinetics parameters was evaluated as well. The study found that the photocatalytic rate has the following form: $R = k_m(C_0 - C_s) = \frac{k[I(\theta),w]KC_s}{1+KC_s}$. Using the same reactor type, Zhou and Ray [26] discussed the degradation kinetics of Eosin B dye. With the application of the dip-coating technique, the P25 catalyst was deposited on a Pyrex glass. With the correction to mass transfer effect, kinetic rate constants were obtained based on various operational factors: catalyst film thickness and light intensity. The influence of different parameters on photocatalytic degradation was evaluated, such as pH, temperature, and dissolved O₂. It was concluded that the degradation kinetics rate constant could be described by the following equation $k_r = \frac{4.3K_s\sqrt{wl}^{0.83}}{1+4.3\sqrt{wl}^{0.83}}$. Hashim et al. [28] used a swirl-flow reactor to explore the photocatalytic degradation of diclofenac (DCF) over a thin film of P25 and modified (doped and sensitized TiO₂). Two different catalysts support: Pyrex glass and fiber glass were used to achieve better immobilization. Under the influence of UV and visible light, the kinetic rate parameters were evaluated, such as pH, flowrate, DCF concentration. Their study indicated that the dye-sensitized TiO₂ has higher degradation rates under visible light than doped TiO₂ and P25 catalysts. In addition, the reaction rate constant had the form: $k_r = 0.92(I)^{0.53}$. Chen et al. [32] investigated the influence of external and internal mass transfer on the photocatalytic degradation of benzoic acid. Using an immobilized P25 catalyst, two different illumination configurations were applied: substrate-catalyst (SC) and liquid-catalyst (LC) illumination. Different factors such as adsorption constant, dynamic adsorption constant, effective diffusivity, and internal and external mass transfer coefficients were evaluated theoretically and experimentally. The impact of catalyst layer thickness on the degradation performance was investigated as well. It was found that the internal mass transfer resistance governs the overall degradation rates. The overall rate reached a saturation value for LC configuration while an optimum thickness was achieved for SC configuration. Zangeneh et al. [33] coated nano TiO₂ particles on quartz tubes and placed them in a photo reactor. Under UV light, the immobilized catalyst was evaluated for linear alkyl benzene (LAB) degradation. To examine the reactor performance, the influence of three independent factors: initial pH, initial chemical oxygen demand (COD), and reaction time, was studied using response surface methodology. The influence of O₃, H₂O₂, and O₃/H₂O₂ on the degradation behavior was also discussed. For the applied range of variables, the optimum conditions were obtained. It was observed that the reactor has an efficiency of 37% for degradation without chemicals' addition. The photocatalytic reaction was enhanced by adding H₂O₂, O₃, and O₃/H₂O₂, and such additions led to obtaining efficiencies of 50, 60, and 69%, respectively. Using titanium butoxide and P25, Arabatzis et al. [34] used two different methods: doctor-blade and dip-coating, for depositing TiO₂ on glass substrates. The thin film's photoactivity was checked for 3,5-dichlorophenol (3,5-DCP) removal. It was

revealed that the degradation registers pseudo first order reaction kinetics. In addition, the thin films of P25 had higher removal rates than the prepared TiO_2 films, while the doctor-blade technique was more successful due to achieving a stable film photoactivity over many operation hours.

In this article, the kinetics of photodegradation of diazo dye, Direct Blue 15 (DB15), over suspended and immobilized P25 catalyst was explored. For different catalyst-placement modes, the experiments of degradation kinetics were carried out in a swirl flow reactor. In terms of slurry catalyst, the pH behavior was initially investigated by conducting different experiments within a broad range of pH values to determine the optimum pH value for dye degradation. The kinetics experiments were then performed at the optimized pH value under the influence of different variables. The influence of different parameters: dye concentration, catalyst loading, and light intensity, on the DB15 kinetics was examined. The kinetics results are evaluated with the application of three different kinetic approaches: k_a pathway, approach of single value of k_r and K and path of k_r as of variable. In the latter approach, the L-H constant k_r is correlated to three different parameters to achieve a mathematical model. Based on the derived formula, the predicted k_a values are then determined and compared with their corresponding lab values. The developed model's validity is also tested by comparing its predicted values with the laboratory values. In addition to the L-H model, the obtained data was entirely fitted using non-linear regression to develop an empirical model with three different variables. The DB15 mineralization was also discussed. For immobilized catalyst mode, P25 was deposited using a dip-coating device. The film's surface characterization was evaluated. The P25 thin films were then studied for DB15 degradation kinetics by evaluating the effect of different operating variables such as light intensity and initial dye concentration. The degradation rate constants were determined based on the k_a approach. The P25 thin film's durability was also checked to evaluate its recyclability.

2. Experimental Details

2.1. Materials

DB15 dye was obtained from Sigma-Aldrich (Oakville, ON, Canada). Commercial P25 powder provided by Degussa company (Germany) was used as a suspended catalyst. The initial pH values were adjusted to the desired values using HNO_3 (70%) (Oakville, ON, Canada) and KOH (Merck, Germany). These chemicals were used as received without further purification. In this study, all dye solutions were prepared with Milli-Q water that also was used for reactor cleaning purposes after each experiment. The chemical structure of DB15 is provided in Figure 1.

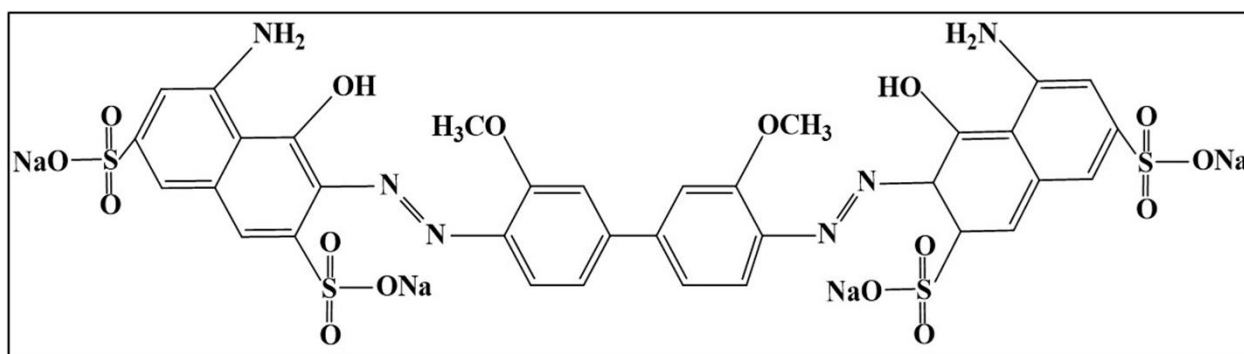


Figure 1. Chemical structure of DB15.

2.2. Swirl-Flow Photoreactor

The photodegradation experiments were performed in a swirl-flow reactor. The reactor is composed of a circular frame made of stainless steel and aluminum except for the reactor's bottom, where a circular glass plate exists inside the frame. Two rubber O-rings

are placed inside the reactor frame at the lower and upper sides of the circular glass plate to protect its vessel from leaks. The reactor is unique in its type due to two-reactor inlets that lead to numerous advantages. Its design allows for providing a high ratio of catalyst surface area to reactor volume; effectively deals with high flow rates with minimum pressure drop values; allows for selection flexibility between suspended and supported catalyst modes; and efficiently evaluates the degradation kinetics concerning different parameters such as liquid flow rate, dye concentration, catalyst loading and light intensity. The photoreactor layout and its details are displayed in Figure 2A. The experimental setup used for the experiments is shown in Figure 2B.

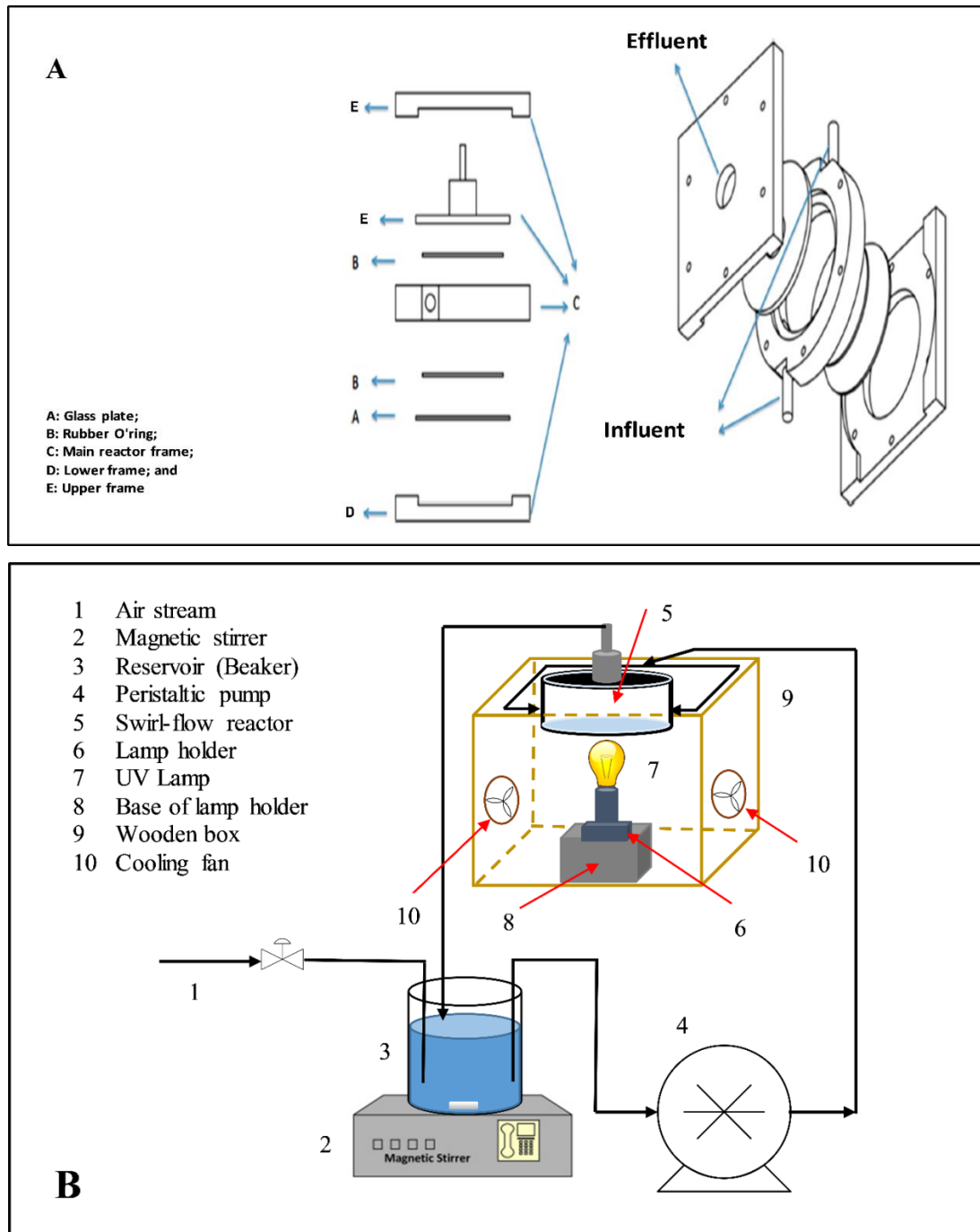


Figure 2. (A) The design layout of the swirl flow photoreactor and (B) A schematic representation of the experimental setup.

With a peristaltic pump, the suspension solution entered the reactor by means of two inlets in opposite directions. The pump was connected to a tank equipped with a magnetic stirrer to achieve homogenous suspension. From the center of the upper frame, the suspension solution left the reactor back to the tank to achieve complete circulation. When the suspension enters via two inlets at different directions, it generates a swirl flow in the reactor resulting in reduced channeling phenomena, minimized dead zones' volume, and enhanced liquid mixing. Thus, mass transfer resistance between different phases: dye solution and catalyst surface is reduced to a minimum level. This results in the adsorption of large amounts of dye molecules on the catalyst surface and, subsequently, increased dye degradation rates. In addition, because the reactor's design provides a high ratio of catalyst surface area to reactor volume, large quantities of light absorbed on the catalyst surface led to increased dye degradation. Based on the above, operational factors such as light intensity, catalyst and dye concentration have a big effect on the swirl-flow reactor performance and dye degradation. Air was entered into the tank via a connection pipe to supply the O₂ required for suspension solutions to ensure continuous oxidation.

Under the influence of UV light, the suspension solutions were irradiated using a UVA lamp (Sylvania–Mercury Vapor Lamp: 175 W). At the bottom of the circular glass plate, the lamp was placed directly under the reactor and was positioned on a holder that could be moved. Thus, the angle of the light incident could be changed accordingly. To minimize the effect of natural light on the experiments, the used lamp, and its holder and the photoreactor bottom frame were positioned in a wooden box. The mentioned box has an inner face covered with foil paper, while its external face has two cooling fans in opposite directions to avoid lamp overheating [28].

2.3. Catalyst Immobilization

2.3.1. Dip-Coating Apparatus

The dip-coating apparatus consists of a vertical structural frame connected to two horizontal frames and a horizontal plate. An electrical motor (Leeson Electric Corporation, WI, USA) with 1 H.P. is placed on the horizontal plate and connected to a lead screw shaft (threaded screw rod) mounted on a ball-bearing at both ends. The screw shaft is vertically positioned between the vertical frame and horizontal plate and fixed using small pins. A sample holder is mounted on the screw shaft using a ball bearing, which conveys through the shaft's level limits. The upper and lower limits of the sample holder, cycle limits, are determined using two position sensors placed on a vertical rod located beside the screw shaft. The position of the mentioned sensors can be adjusted based on the cycle level requirements. Under the horizontal plate, a movable horizontal frame includes four heat lamps (175 W, Philips, Markham, ON, Canada) distributed in different directions; thus, the horizontal plate's height can be adjusted. Additionally, the position of the heat lamps can be relocated according to the coating requirements. The lower horizontal frame includes four wheels so that the device can be moved easily between different places. The purpose of this frame is to provide support for the device. The dip-coating device was built by the University Machine Shop (UMS) previously used by our group (e.g., [28]) and was initially designed for tube coating. Therefore, the device is modified before it is used in the circular glass coating. The modification includes a cylindrical shaft connected to a circular frame. The rod well fits the sample holder of the device while the circular glass is placed on the circular frame and is fixed by four small nuts and bolts. The details of the dip-coating device and its modification are presented in Figure 3 [35].

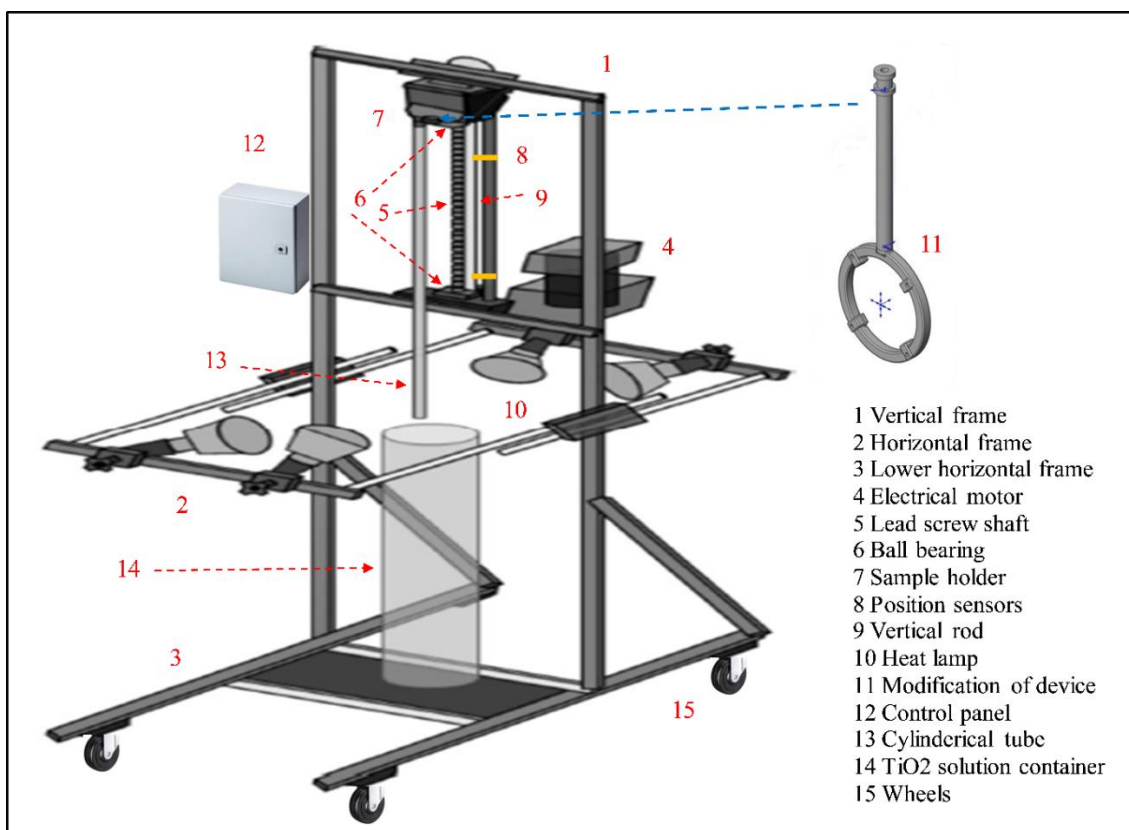


Figure 3. Dip-coating device details.

2.3.2. Catalyst Immobilization Procedure

The Pyrex glass was first sandblasted to increase the surface roughness and enhance the strength of catalyst fixation. The Pyrex glass was then soaked in a 5% Nitric acid solution overnight to remove fragile surface parts created due to the sandblasting process. To minimize the acidic solution's influence, the Pyrex glass was rinsed many times with MQ water then was dried in an oven at 105 °C. An appropriate amount of TiO₂ was added to MQ water to achieve a 1.5% catalyst concentration. The solution was then sonicated using an ultrasonic cleaner (model F560, Fisher Scientific, Ottawa, ON, Canada) for 1 h, resulting in a milky solution [28]. The milky solution was stirred at 200 rpm using a mixer (IKA Eurostar, IKA Works Inc., Wilmington, NC, USA) for about 30 min to obtain better homogeneity. After the milky solution was prepared, the Pyrex glass was inserted into the milky solution and pulled out at a dipping speed of about eight mm/s using the dip-coating device. The coated thin film was dried in an oven at 100 °C for 1 h to remove the water content. To keep the coated film from cracking, the coating catalyst was then calcined in a vacuum oven for 0.5 h at 250 °C with a low-temperature ramp of about 0.03 °C/s under a vacuum pressure up to about −0.15 bar. Under the same vacuum pressure range, the thin film was cooled down to room temperature, about 21 °C. The cooling down of the thin film temperature under a controlled vacuum pressure ensured a fixed temperature reduction. Thus, the presence of film cracking was avoided. The entire procedure mentioned above was repeated depending on the required film thickness. To determine the amount of coated catalyst, the glass substrate was weighed before and after the coating process.

It is important to mention that the swirl flow reactor includes two rubber O-rings on both sides of the reactor housing to seal the reactor from any possible leakage. The presence of those O-rings leads to cover circular parts of the glass and create a shaded area on both sides of the reactor frame because of cutting off the emitted light from the lamp. Thus, it is assumed that there are no sufficient photoreactions over the created shaded area compared to uncovered areas. Based on this, reducing the coating area to the actual area

of those O-rings is quite reasonable to maximize the light distribution per the coated area and lower the related cost of TiO_2 amount reduction. To achieve this objective, a similar rubber O-ring is placed on the modified circular frame of the dip-coating device during the coating process to simulate the reactor during its normal operation. A schematic diagram of the approach used for the Pyrex glass coating is presented in Figure 4. Additionally, one face of the circular frame was covered using parafilm and heat tape as the coating of one glass face is required. For the same reason, two heat lamps instead of four lamps were used for quick drying during the coating process.

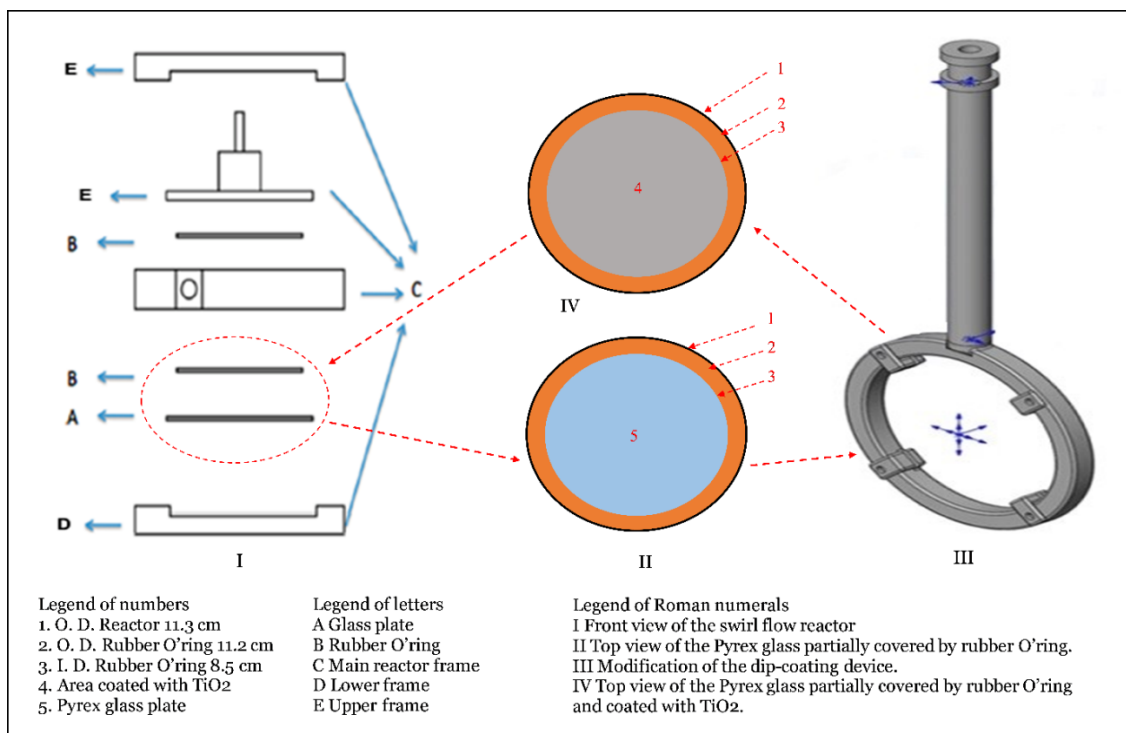


Figure 4. A graphical representation of the approach used for the Pyrex glass coating.

2.3.3. Surface Characterization of Thin Film

The thin film's surface characterization at the maximum amount of coated TiO_2 was investigated at the Western Nanofabrication Facility at Western University. Morphological properties: surface morphology and texture were studied by scanning electron microscopy (SEM) using a microscope LEO (Zeiss) 1540 XB FIB/SEM. The thin film of TiO_2 was analyzed at an accelerating voltage of 6 kV, with different working distances and magnification factors. Prior to analysis, the film was dried and coated with a thin layer of conductive material (Osmium) using an Osmium Plasma Coater (Filgen OPC80T).

2.4. Photodegradation Experiments

For slurry catalyst experiments, the numbers of tested variables were reduced to achieve to save time and cost. To this end, all experiments were carried out at room temperature and a constant liquid flow rate (2.1×10^{-2} L/min). Firstly, the impact of initial pH on the DB15 removal was examined to determine an optimum value. The pH values were varied from 3 to 9 while keeping other conditions constant: catalyst concentration 0.5 g/L, light intensity 11.2 W/m^2 , and two different dye concentrations of 25 mg/L.

Once the pH value was determined, a group of experiments was performed at the optimized pH value to investigate the kinetics of DB15 degradation. The influence of dye concentration and catalyst loading on the degradation kinetics was examined. The kinetics experiments were conducted within a catalyst loading and dye concentration ranged between 0.2–1.5 g/L and 15–60 mg/L, respectively, at two different light intensities, 9.7 W/m^2

and 11.2 W/m². The impact of light intensity on the reaction kinetics was evaluated as well. A set of experiments were performed at different light intensities to achieve this, ranging from 1 to 11.2 W/m². The mineralization runs were conducted at natural pH, dye concentration 40 mg/L, light intensity 11.2 W/m², and catalyst loading ranged between 1–2 g/L. The Total Organic Carbon (TOC) of DB15 solutions was determined at various reaction times to evaluate the dye mineralization.

For the immobilized catalyst experiments, the kinetics experiments were performed at natural pH by examining the influence of light intensity and dye concentration on the degradation performance. The dye concentration ranged between 9–25 mg/L, while the extent of light intensity ranged from 1 to 11.2 W/m². The thin film durability was evaluated as well. To achieve the objective, a group of experiments was conducted at a dye concentration of 13 mg/L to examine the P25 film recyclability. After each experiment, the reactor was cleaned, and the dye solution was removed using MQ water. An amount of fresh MQ water was then circulated through the reactor while the UV light was on for half an hour to remove any remaining adsorbed dye molecules from the catalyst surface. After that, the immobilized catalyst was dried in an oven at 110 °C for 3 h.

2.5. Analytical Methods

In this research, DB15 dye solutions with a volume of 250 mL were prepared using Milli-Q water and the corresponding amount of DB15 dye to obtain the desired concentration. For slurry catalyst experiments, the solution pH was measured by a pH meter (Metrohm 780, Riverview, FL, USA). Depending on experiment requirements, the light intensity values were changed by placing different wire mesh sizes between the circular glass plate and the lamp. The light intensity values were measured on a UVX digital radiometer (E28310, Fisher Scientific). At regular time periods, samples of dye mixture about 5 mL were collected from the tank using a syringe and filtered through Polypropylene Millipore filters (0.45 µm) (VWR, Edmonton, AB, Canada). The filtered samples' absorbance was measured on a UV-Vis spectrophotometer (UV-3600, Shimadzu, Japan) by recording their spectrum from 300 to 800 nm. The decolorization of dye solutions was evaluated from their maximum absorbance at 598 nm [36] by converting absorption to concentration through a calibration curve that was prepared earlier than dye degradation experiments. The efficiency of dye removal was calculated as follows:

$$\text{Dye removal (\%)} = \frac{C_0 - C_t}{C_0} \times 100 \quad (3)$$

where C_0 and C_t are the DB15 concentrations at time 0 and t , respectively.

For the TOC test, samples of about 5 mL were taken using a syringe, filtered (0.45 µm) and assessed using a Shimadzu TOC-V CPN analyzer (Shimadzu, Japan). The obtained findings were then used to evaluate the dye mineralization as a percentage of carbon removal for TOC measurements.

3. Results and Discussion

3.1. pH Optimization

The behavior of DB15 degradation within a wide range of pH values is displayed in Figure 5A,B. As shown in Figure 5A, a low degradation rate is observed at pH 9 (pH higher than pzc range values). This outcome is mainly due to a repulsive force between the negatively charged Degussa surface and anionic DB15 dye that includes four negative sulfonate groups. Such a repulsive force leads to adsorb little amounts of DB15 on the P25 catalyst surface, subsequently a lowered removal rate. As the pH values decrease and become lower than pzc range values, the DB15 removal is increased. This behavior is explained by the presence of a strong attractive force between anionic DB15 and the positively charged Degussa surface, which results in the adsorption of large amounts of DB15 on the catalyst surface. Hence, the degradation rate is then increased.

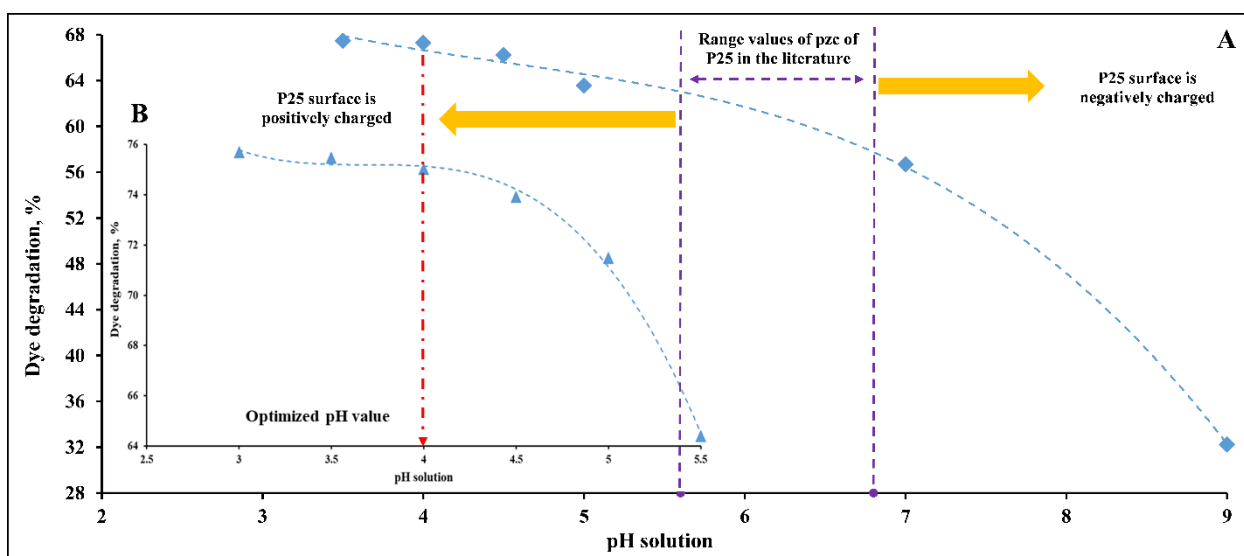


Figure 5. pH optimization for DB15 degradation at catalyst concentration 0.5 g/L, light intensity 11.2 W/m² and two different dye concentrations: (A) Dye concentration 25 mg/L, (B) Dye concentration 20 mg/L.

It is important to note that the degradation rate was negligibly increased, approximately stable at pH 4. Similar behavior was reported for Metanil Yellow dye, mono azo, with one sulfonate group. Such behavior was justified within pH values ranged between the pzc of Degussa and pH 4 [4]. It was clarified that the continuous decrease in pH values leads to adsorb large amounts of dye molecules because of the significant increase in the attractive force. Thus, a reduction would be registered in the free active sites and the amount of absorbed light on the Degussa surface. Hence, the dye removal is slowed down correspondingly.

More importantly, because getting higher removal rates is desirable, lower pH is preferred, more specifically, the pH values below the pzc point (value of 5.6). This ensures a strong attractive force that leads to the adsorption of large amounts and, subsequently, more dye degradation. Therefore, Figure 5B focuses on the pH values that ranged between 3 and 5.5. Interestingly, a similar trend is registered for DB15 degradation though different dye concentration was used. According to this discussion, the value of pH 4 was selected as the optimal value for the experiments of degradation kinetics. Further details can be found in [37].

3.2. Degradation Kinetics

It has been widely reported that the photocatalytic degradation rate of different organic compounds usually follows the L-H model [11–16,38,39]. The equation for the widely accepted L-H model for photocatalytic degradation rate shown in Equation (4) is presented below in terms of DB15:

$$r_{\text{DB15}} = -\frac{dC_{\text{DB15}}}{dt} = \frac{k_r K \cdot C}{1 + K \cdot C} \quad (4)$$

3.2.1. Approach of k_a Model

It is known that the concentration of a pollutant has a big effect on the wastewater treatment process. Thus, it is important to evaluate the influence of initial dye concentration on the degradation kinetics [40]. At low dye concentrations, the integration of Equation (1) leads to a pseudo first-order kinetics reaction [13,15,17].

$$\ln \frac{C_0}{C} = k_r K \cdot t = k_a \cdot t \quad (5)$$

A plot of $\ln\left(\frac{C_0}{C}\right)$ vs. time gives a straight line, and its slope from linear regression represents the value of k_a . This approach is considered the main path for evaluating dye degradation kinetics, followed by many researchers [20–24,30,40]. In this path, k_r and K are lumped together as one parameter. The outcomes of DB15 kinetics experiments at different dye concentrations are presented in Figure 6 and Table 1. The results show that linear fit with high correlation coefficient (R^2) values were achieved for all the examined concentrations. This indicates that the pseudo first-order model well described the kinetics of DB15 degradation. As can be seen in Table 1, the k_a value decreases when the DB15 initial concentration is increased. The k_a was highly reduced to 10.85×10^{-3} from $75.74 \times 10^{-3} \text{ min}^{-1}$ as the DB15 concentration increased from 15 to 60 mg L^{-1} . The reason for such a decrease in k_a values is discussed below in detail.

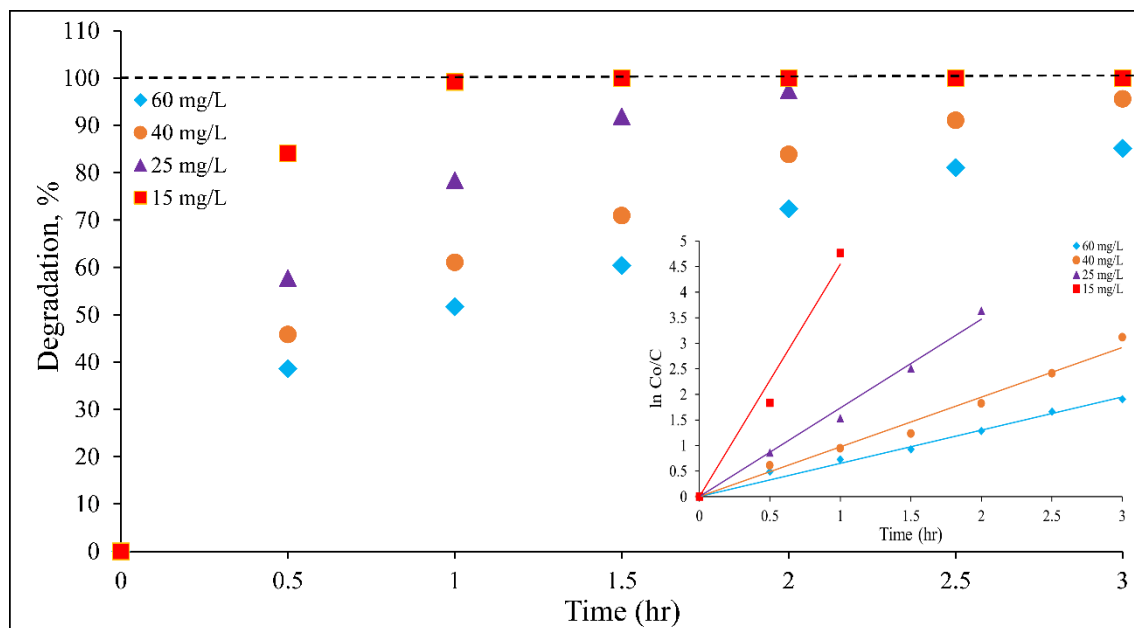


Figure 6. Kinetics of DB15 degradation at different dye concentrations (pH 4, catalyst loading 1 g/L, and light intensity 11.2 W/m^2).

Table 1. Kinetics data obtained at pH 4 and different reaction conditions.

N	Dye Concentration (mg/L)	Catalyst Loading (g/L)	Light Intensity (W/m^2)	$k_a \times 10^3$ (min^{-1})	R^2
1	60	1	11.2	10.85	0.9857
2	40	1	11.2	16.22	0.9823
3	25	1	11.2	28.89	0.9905
4	15	1	11.2	75.74	0.9796
5	36	0.2	9.7	6.03	0.9912
6	36	0.4	9.7	7.81	0.9846
7	36	0.8	9.7	11.44	0.9946
8	36	1.5	9.7	21.2	0.9789
9	20	1	1	4.39	0.9802
10	20	1	2.5	13.57	0.9965
11	20	1	6.1	26.68	0.995
12	20	1	11.2	48.12	0.9886

As the dye concentration increases, more dye molecules would be adsorbed on the catalyst surface. Hence, the number of accumulated dye molecules becomes higher than the degraded molecules that leave the surface. Such accumulation leads to catalyst surface saturation, and the dye molecules in the bulk solution cannot reach the surface. Thus, the accumulated molecules play an inhibitory role in dye degradation, which results in

slowing down the dye removal [15,40]. In addition, the concentration increases lead to the generation of more by-products depending on the increase rate. Thus, competitive adsorption occurs between the increasing number of intermediates and dye molecules on the catalyst surface. This results in lowering the active sites available for hydroxyl ions adsorption, and the generation of hydroxyl radicals would be therefore reduced [15,27,30]. Furthermore, while the dye concentration is increased, the solution permeability to UV light decreases correspondingly. Hence, the photons' path length is affected due to a light penetration difficulty, and their number would be decreased, resulting in a reduction in the dye photodegradation [15,17,27,30,40,41].

Under the effect of different catalyst loadings and various light intensities, DB15 kinetics exhibit similar behavior. As shown in Table 1, the k_a values are proportional to the catalyst loadings and light intensities in which k_a increases when these parameters are increased. Based on the above, it can be concluded that the L-H model appears to fit well with the experimental results.

From this path, the obtained data can be further analyzed using the half-time approach as explained in the following discussion. The formula of Equation (1) can be rearranged and simplified to Equation (6) [17,19,40–42].

$$\frac{1}{k_a} = \frac{1}{k_r \cdot K} + \frac{C_o}{k_r} \text{ or } \frac{1}{r} = \frac{1}{k_r \cdot K C_o} + \frac{1}{k_r} \quad (6)$$

By plotting the obtained $(1/k_a)$ values vs. different initial dye concentrations using Equation (6), the k_a dye concentration-dependent equation is achieved. The slope of the equation is equal to $(1/k_r)$ while the intercept is equal to $(1/k_r \cdot K)$. The values of k_r and K were $0.574 \text{ min}^{-1} \text{ mg L}^{-1}$ and 0.165 L mg^{-1} , respectively. The mentioned values represent the approach of single value of k_r and K , as it will be discussed later. However, their use in the half time equations is the main purpose of obtaining these values in this part.

After rearrangement, the integration of Equation (6) leads to Equation (7). By inserting the k_r and K values and the dye concentration reaching half of its initial concentration, the equation of estimated $t^{1/2}$ values can be written as shown in Equation (8) [40,42]. Meanwhile, the equation of observed $t^{1/2}$ values is obtained from Equation (2) as presented in Equation (9) [24,40,42]. The estimated and observed $t^{1/2}$ values are presented in Table 2. It was proposed that the generated intermediate products at high dye concentrations compete with the original dye molecules for a limited number of active sites on the catalyst surface, resulting in a delay of the half-times required for the dye degradation [40,42,43].

$$t = \frac{1}{k_r K} \ln \frac{C_o}{C} + \frac{1}{k_r} [C_o - C] \quad (7)$$

$$\text{Estimated } t^{1/2} = \frac{\ln 2}{k_r K} + \frac{0.5 C_o}{k_r} \quad (8)$$

$$\text{Observed } t^{1/2} = \frac{0.693}{k_a} \quad (9)$$

Table 2. The estimated and observed $t^{1/2}$ values at different dye concentrations.

Co mg/L	$k_a \times 10^3 \text{ min}^{-1}$	Estimated $t^{1/2}$ min	Observed $t^{1/2}$ min
60	10.85	59.58	63.87
40	16.22	42.16	42.73
25	28.89	29.09	23.99
15	75.74	20.38	9.15

As a result, it can be stated that though this path is reliable and acceptable for many researchers, it has drawbacks. Because the approach deals with a single parameter, the influence of tested factors totally ignores their impact on its individual parameters, k_r and

K. Hence, the response of the k_a constant to the group of applied factors is considered an aggregate response. It does not reflect the real effect of those examined factors on the above-mentioned two individual parameters, registering a lack of validity.

3.2.2. Single Value of k_r and k

The concept of this approach is mainly built on finding individual values for both k_r and K constants [17,42]. Hence, this path is more specific than the previous approach in terms of evaluating the required constants. With Equation (6), the plot of $(1/k_a)$ values vs. different concentrations results in achieving the k_a dye concentration-dependent equation as shown in Figure 7. From the mentioned figure, the equation's slope and intercept are obtained, equivalent to $(1/k_r)$ and $(1/k_r \cdot K)$. Hence, the k_r and K were determined, and their values were $0.574 \text{ min}^{-1} \text{ mg L}^{-1}$ and 0.165 L mg^{-1} , respectively. In the current case, dye concentration changed from 15 to 60 mg L^{-1} . Therefore, the path completely ignores the influence of different factors on the mentioned constants, resulting in a considerable deficit in its validity and reliability.

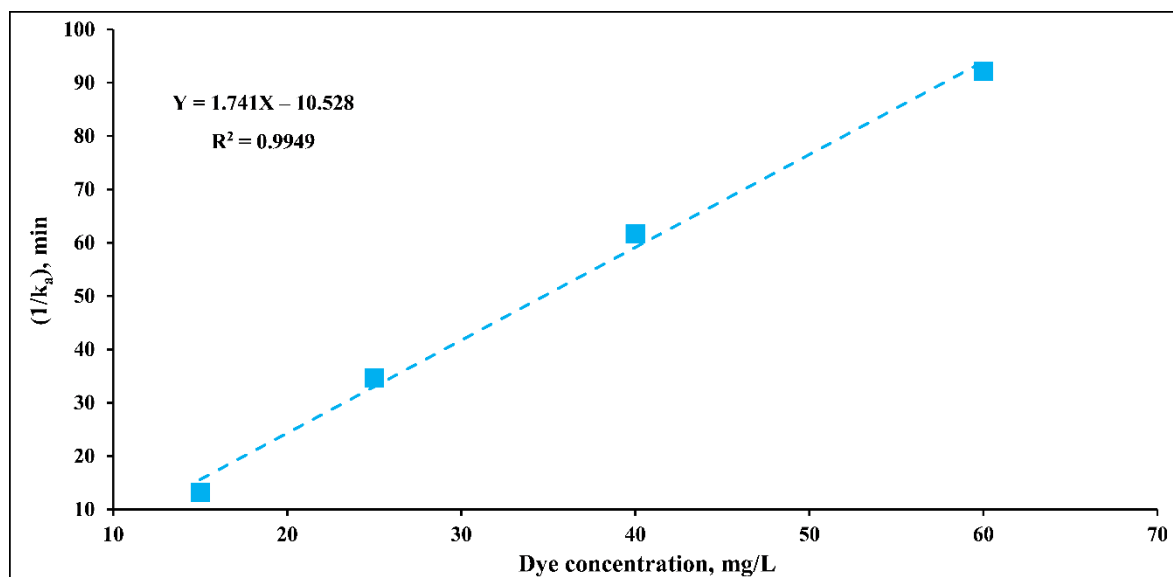


Figure 7. Influence of different dye concentrations on the k_a constant of DB15 degradation at the conditions: pH 4, catalyst loading 1 g/L , and light intensity 11.2 W/m^2 .

3.2.3. Approach of k_r as of Variable

This path deals with k_r as a variable for different factors. Thus, this approach considers the influence of different parameters such as initial dye concentration and light intensity on k_r . In terms of DB15, the general equation of the L-H model can be written as follows:

$$r = -\frac{dC_{\text{DB15}}}{dt} = \frac{k_r \cdot KC}{1 + KC_0} \quad (10)$$

Earlier, Al-Ekabi and Serpone [23] and Augugliaro et al. [44] suggested that the term competitive adsorption of intermediate compounds should be included within the rate equation. This suggestion has been followed by many researchers [42,45]. After adding the competitive adsorption term, the rate equation becomes as shown in Equation (11). Al-Ekabi & Serpone [23] and Augugliaro et al. [44], then followed by Chen & Ray [45], made the following assumption (Equation (12)):

$$r = -\frac{dC}{dt} = \frac{k_r \cdot KC}{1 + KC + \sum K_1 C_1} \quad (11)$$

where K_I and C_I are the adsorption constant and concentration of intermediate compounds.

$$KC + \sum K_I C_I = KC_o \quad (12)$$

It is important to mention that the approximation applied to relatively lower molecular weight compounds [23,44,45]. The use of such model compounds leads to generate a lower number of intermediate compounds. Thus, the approximation appears to be quite reasonable. The application of such an approximation with higher molecular weight compounds (e.g., DB15 with a M.W. of $\cong 993$) is still questionable due to the generation of a large number of side-products that can theoretically compete with the original dye to adsorb on the catalyst surface, especially at earlier stages of the reaction. However, it has been previously reported that the mentioned approximation is used for organic compounds with relatively higher molecular weights [27,46]. By inserting Equation (12) into Equation (11), the following equation is obtained.

$$r = -\frac{dC}{dt} = \frac{k_r \cdot KC}{1 + KC_o} = k_a \cdot C \quad (13)$$

From Equation (13), the formula of k_a can be written as follows [27,46]:

$$k_a = \frac{k_r \cdot K}{1 + KC_o} \quad (14)$$

From the approach of a single value of k_r and K , it was obtained earlier that the value of K is 0.165 L mg^{-1} . It has been previously reported that K is an independent parameter. It refers to an organic pollutant's adsorptive affinity on a solid surface, precisely, catalyst surface [25]. Thus, it considers as a characteristic property for a particular pollutant type. However, such specific property may be quite different among various pollutant types. Based on this, the K is considered as a constant value for this model. With the application of the K value, k_a values are fitted to different initial DB15 concentrations (Equation (14)); thus, k_r values are obtained as shown in Table 3.

Table 3. Langmuir-Hinshelwood constant (k_r) values at different initial dye concentrations.

Concentration mg/L	Rate Constant $k_r, \text{ mg L}^{-1} \text{ min}^{-1}$
60	0.716
40	0.747
25	0.897
15	1.595

By plotting the obtained k_r values (Table 3) vs. different dye concentrations, the k_r initial dye concentration-dependent equation is achieved. Then, the best-fit equation can be obtained by applying non-linear regression using the MINITAB software package (Version 19.2020.1) (Minitab, LLC, State College, PA, USA). The actual values and their best-fit equation of k_r for the range of dye concentrations are shown in Figure 8 and Equation (15), respectively.

$$k_r = 9.86 [C]_o^{-0.69} \quad (15)$$

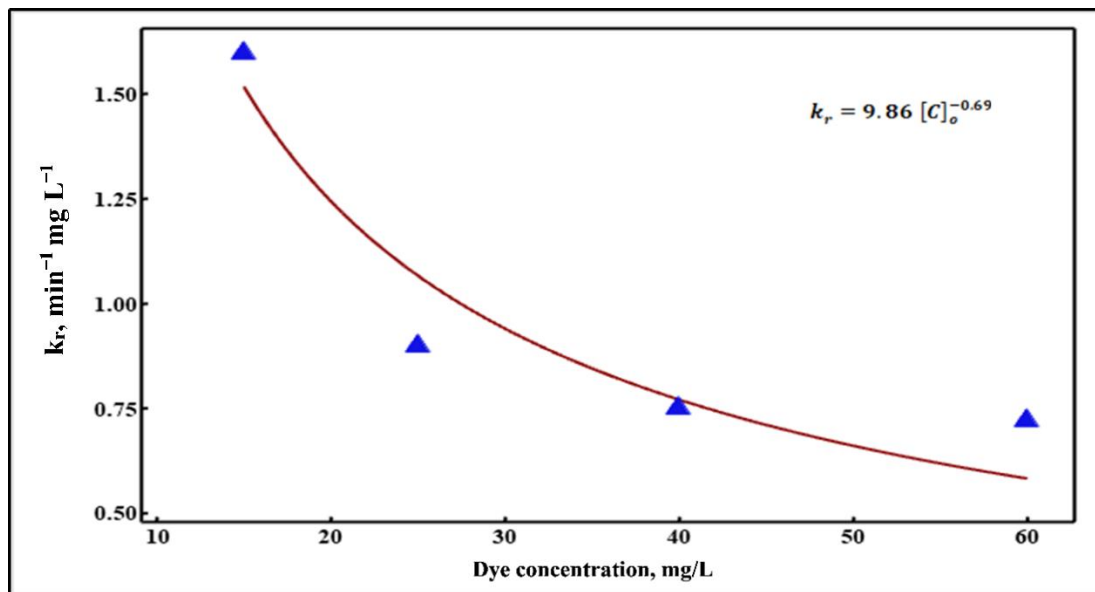


Figure 8. Non-linear regression of k_r values vs. different dye concentrations.

Following the same procedure, the values of k_r are obtained by fitting k_a values to different catalyst loadings and various light intensities; their obtained values are shown in Tables 4 and 5, respectively.

Table 4. Langmuir-Hinshelwood constant (k_r) values at different catalyst loadings.

Catalyst Loading g/L	Rate Constant k_r , $\text{mg L}^{-1} \text{min}^{-1}$
0.2	0.254
0.4	0.328
0.8	0.481
1.5	0.892

Table 5. Langmuir-Hinshelwood constant (k_r) values at various light intensities.

Light Intensity W/m^2	Rate Constant k_r , $\text{mg L}^{-1} \text{min}^{-1}$
1	0.114
2.5	0.354
6.1	0.695
11.2	1.254

The plotting of the obtained k_r values (Table 4) vs. different catalyst loadings leads to obtaining the k_r catalyst loading-dependent equation. Similarly, the k_r light intensity-dependent equation is achieved by plotting their values (Table 5) vs. various light intensities. With the application of non-linear regression using the MINITAB 19 software package (Version 19.2020.1) (Minitab, LLC, State College, PA, USA), the best-fit equations of these values are then determined. The k_r actual values and their best-fit equations for the range of catalyst loadings and light intensities are presented in Figures 9 and 10, respectively. The best-fit equations of k_r as a function of catalyst loading and light intensity are displayed in Equations (16) and (17), respectively.

$$k_r = 0.64 [W]^{0.73} \quad (16)$$

$$k_r = 0.14 I_0^{0.91} \quad (17)$$

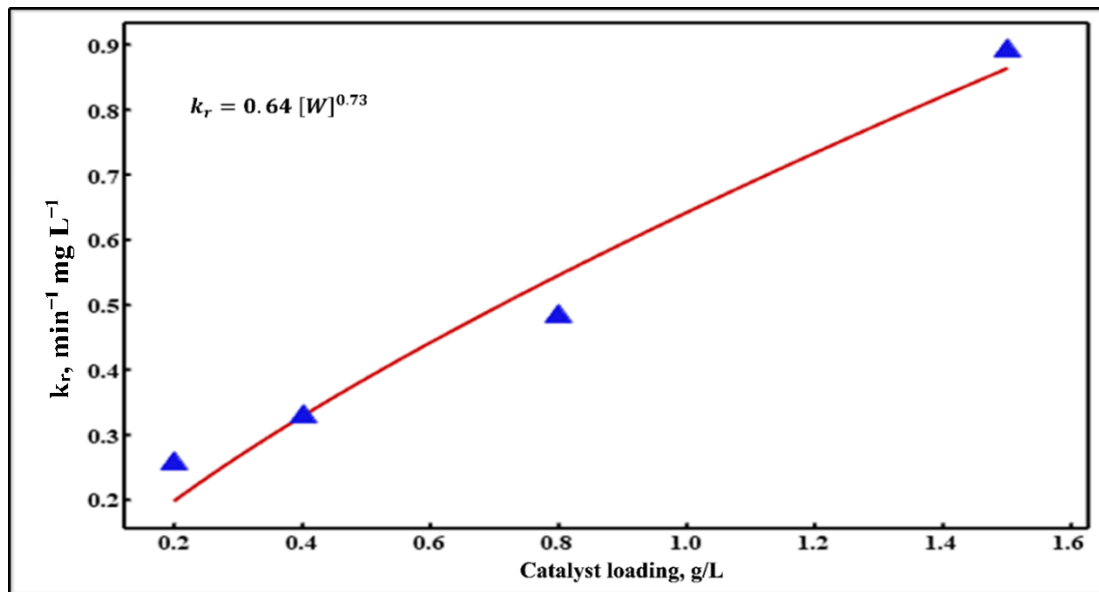


Figure 9. Non-linear regression of k_r values vs. various catalyst loadings.

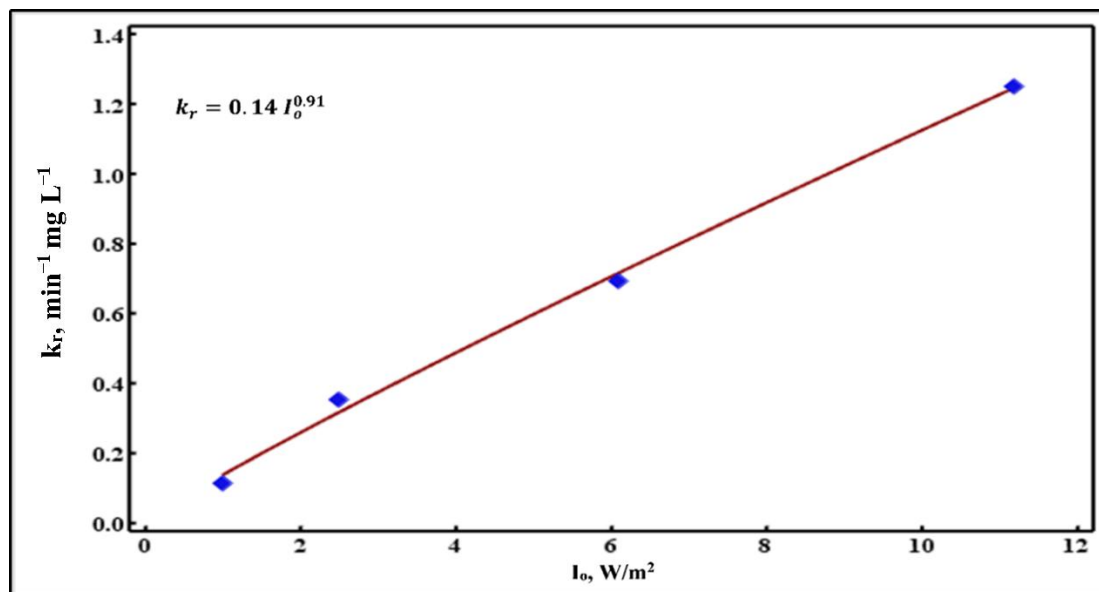


Figure 10. Non-linear regression of k_r values vs. different light intensities.

By inserting Equations (15)–(17) into Equation (14), the following equation is obtained:

$$k_a = \frac{0.15 [C]_0^{-0.69} [W]^{0.73} I_0^{0.91}}{1 + 0.17 [C]_0} \quad (18)$$

To examine the model's validity, a comparison between experimental and predicted k_a values for all obtained data is evaluated in Figure 11. The predicted values are determined using the developed model equation, while the observed values are obtained from the experimental results. As shown in Figure 11, it is noted that the model data trends to fitting well the results of kinetics experiments, indicating a good agreement between both theoretical and practical sides. Based on the above, the developed model is quite reasonable in reflecting the extent of experimental observations, referring to achieving good credibility.

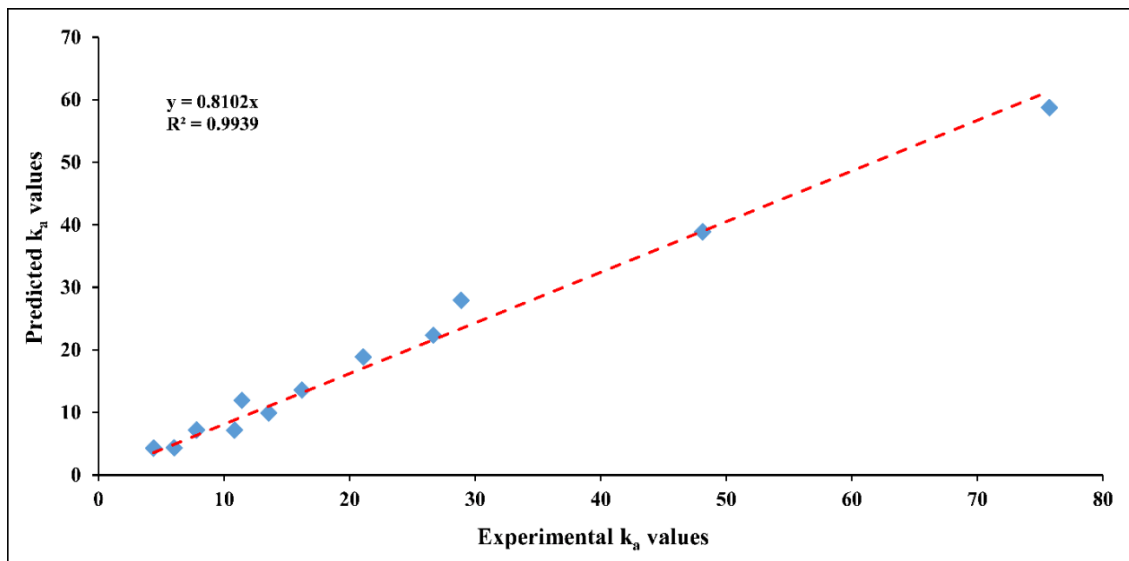


Figure 11. A comparison between experimental and predicted ($k_a \times 10^3$) values for different operating conditions.

3.2.4. Empirical Model

Power-Law Kinetic Model

As mentioned earlier, the DB15 degradation fits well with the pseudo first order kinetic model (k_a model). Based on Table 1, k_a appears to be a function of three independent variables: dye concentration, catalyst loading, and light intensity. Thus, an empirical model could be developed to examine the impact of the mentioned independent variables on k_a , reflecting the entire experimental data. With the use of non-linear regression analysis, an empirical kinetic model expressed as a power-law equation was developed, as shown in Equation (19).

$$k_a = a [C]_o^b [W]^d [I_o]^e \quad (19)$$

The model's coefficient values were calculated using the MINITAB 19 software package (Version 19.2020.1) (Minitab, LLC, State College, PA, USA). The model constants are distributed as one constant term and three power-law coefficients for each of the independent variables and tabulated in Table 6. By inserting the model's constants into Equation (19), the empirical kinetic model is achieved for predicting k_a values within the operating conditions range as presented in Equation (20).

$$k_a = 0.77 [C]_o^{-1.65} [W]^{0.73} I_o^{0.89} \quad (20)$$

Table 6. Non-linear regression coefficients of the empirical power law kinetic model.

Coefficient	Type	Value
a	Constant term	0.28
b	Power law term	−1.65
c		0.73
d		0.89

Using the empirical kinetic formula, the predicted k_a values were calculated for various experimental conditions. The predicted k_a values were then compared with their corresponding experimental values to assess the empirical model's credibility, as shown in Figure 12. For the range of the tested parameters, it is observed that the data tendency of the empirical model shows a good fit with the experimental data. This indicates a good agreement between the predicted and experimental k_a values, confirmed by the high value of R-squared. According to Figure 12, the proposed empirical model seems acceptable

for considering the experimental data related to the influence of the three independent variables on k_a values with good reliability.

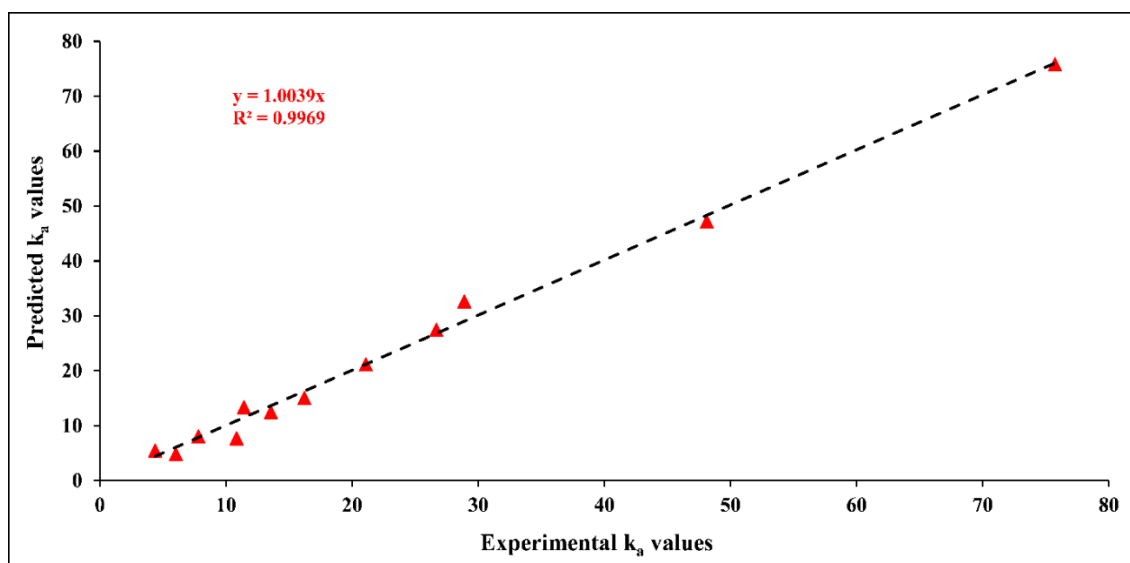
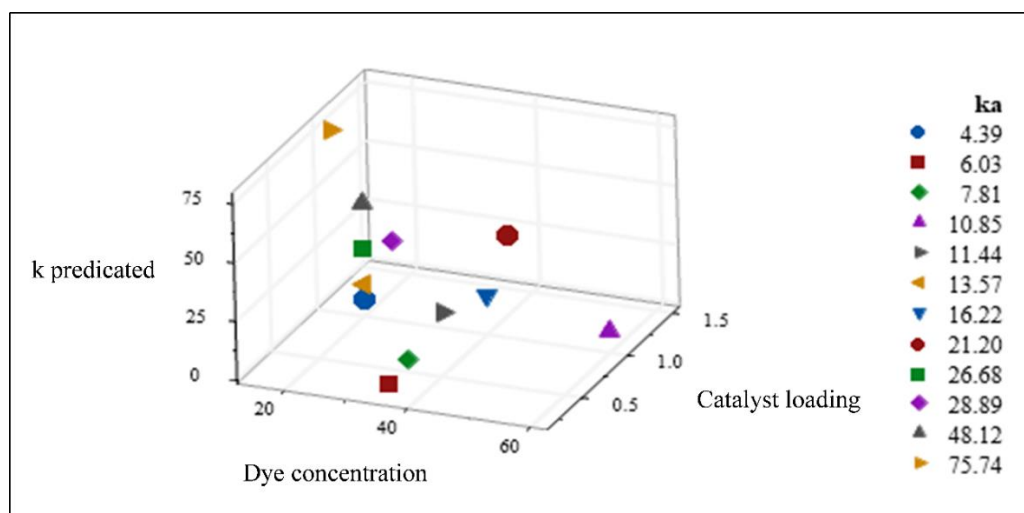


Figure 12. A comparison between experimental and predicted ($k_a \times 10^3$) values for the empirical power law kinetic model.

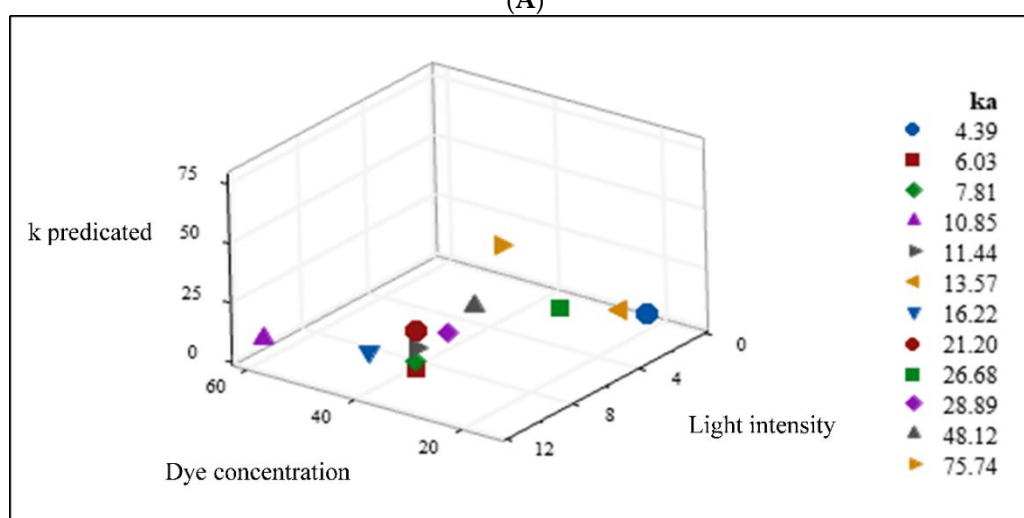
3D Scatterplots

To obtain more understanding, the predicted k_a values using the empirical model are evaluated in terms of the 3D scatter plot's perspective. It is known that a scatter plot refers to a kind of plot that displays data values in the domain of two coordinates, while a 3D scatter plot shows the set of data in three dimensions. Based on this, the predicted k_a values obtained by the empirical model are represented as 3D scatter plots. The 3D graphs are generated, in which the predicted k_a values are a function of two variables among the three independent variables and are displayed in Figure 13A–C.

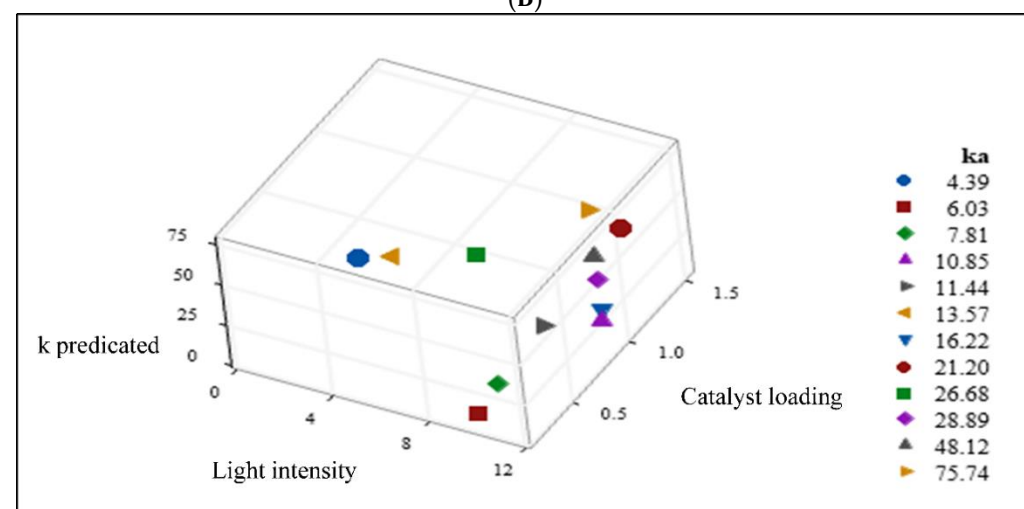
Figure 13A demonstrates the predicted k_a values as a function of dye concentration and catalyst loading. At constant catalyst loading, it is noticed that the predicted k_a value increases as the dye concentration is decreased. This indicates a downhill pattern and negative correlation between the dye concentrations and the predicted k_a values. Numerically, the predicted k_a value is only $7.7 \times 10^{-3} \text{ (min}^{-1}\text{)}$ for a dye concentration of 60 mg L^{-1} , while its predicted value is significantly increased to $75.81 \times 10^{-3} \text{ (min}^{-1}\text{)}$ when the dye concentration reaches 15 mg L^{-1} . Meanwhile, there is a proportional increase in the predicted k_a value when there is an increase in the catalyst loading at constant dye concentration. This results in an uphill pattern and a positive correlation between the catalyst loading and the predicted k_a values. Concerning values, the predicted k_a value increases from $4.86 \times 10^{-3} \text{ (min}^{-1}\text{)}$ to $21.15 \times 10^{-3} \text{ (min}^{-1}\text{)}$ when the catalyst loading is increased from 0.2 gL^{-1} to 1.5 gL^{-1} . As a result, Figure 13A includes two opposite behaviors: downhill and uphill pattern with two different correlations; and negative and positive regarding the influence of dye concentration and catalyst loading, respectively, on the k_a values.



(A)



(B)



(C)

Figure 13. (A) 3D Scatterplot of predicted k_a values obtained by the empirical model vs. dye concentration and catalyst loading. (B) 3D Scatterplot of predicted k_a obtained by the empirical model vs. dye concentration and light intensity. (C) 3D Scatterplot of predicted k_a obtained by the empirical model vs. light intensity and catalyst loading.

Figure 13B presents the predicated k_a values as a function of two independent variables: dye concentration and light intensity. When the dye concentration is stable, a big change is registered in the k_a values for the applied light intensity range. As the light intensity increases, a corresponding increase is achieved in the k_a value, indicating an uphill pattern and a positive correlation. Such correlation describes the relationship between the variable of light intensity and the response k_a at applied conditions. While the k_a registers a value of 5.49×10^{-3} (min^{-1}) at a light intensity of 1 Wm^{-2} , its value is drastically increased to 47.16×10^{-3} (min^{-1}) for a light intensity of 11.2 Wm^{-2} . In contrast, the dye concentration has a behavior of a downhill pattern and a negative correlation with the predicted k_a values, as explained earlier in Figure 13A. Based on this, Figure 13B has two inverse relationships with different behaviors. While a downhill pattern describes the dye concentration relation, an uphill pattern characterizes the light intensity correlation with the predicted k_a values' response. Thus, Figure 13B is similar to Figure 13A in terms of having two opposite patterns and inverse correlations. Figure 13C demonstrates the predicted k_a values as a response to two different factors: light intensity and catalyst loading. It is important to mention that similar behavior is obtained for both light intensity and catalyst loading regarding their effect on the predicted k_a values. An uphill pattern is registered for both the mentioned parameters, indicating a positive correlation between them and the predicted k_a values. Hence, the behavior of these parameters contrasts with the behavior obtained in both Figure 13A,B.

3.3. Comparison of Kinetic Models

To achieve greater understanding, the developed model formulas are compared with some available models in the literature. Table 7 reveals different models have been developed for k_a , K and k_r . It is demonstrated that the evaluation of K and/or k_r as a function of two different variables was rarely reported in literature studies. Thus, the evaluation of K and/or k_r as a function of three independent variables could consider as a good contribution. More importantly, the examination of K and/or k_r at constant pH value has not been assessed to the best of the authors' knowledge. Such evaluation at a constant pH value provides a more in-depth vision of how the mentioned K and/or k_r are affected by different parameters. This is due to the pH's great importance and its governing role on the pollutants' adsorption and catalysts' surface properties. In addition, the discussion of degradation kinetics in terms of initial rates has been widely discussed. However, obtaining initial rate equations of a pollutant as a function of three operational parameters has not been addressed in the relevant literature. This is to the best of the authors' knowledge.

Table 7. Some available k_a , K and k_r models in the relevant literature in comparison with the obtained kinetic models.

N	K	k_r	k_a	Model Compound	Catalyst	Author	Year	Remarks
1	Values ranged 3.46 to $12.6 \times 10^4 \text{ dm}^3 \text{ mol}^{-1}$	Values ranged 2.11 to $4.46 \times 10^{-6} \text{ mol dm}^{-3} \text{ min}^{-1}$	-	Acetophenone	Slurry P25 TiO ₂	Xu & Langford [19]	2000	K and k_r obtained at different I_0 .
2	$0.035 I_0^{0.5} + 0.03$	$0.06 I_0^{0.5}$	-	Para-chlorobenzoate	Slurry P25 TiO ₂	Meng et al. [18]	2002	K and k_r obtained at different I_0 . The correlation equation between their values and I_0 obtained.
3	-	$\frac{4.3 k_s \sqrt{w} I_0^{0.83}}{1 + \sqrt{w} I_0^{0.83}}$	-	Eosin B	Immobilized P25 TiO ₂	Zhou & Ray [26]	2003	k_r obtained as a function of I_0 and W .
4	-	-	$0.0283 [W]^{0.6}$ $72.45 [C]_0^{-1.5}$ $0.03 I_0^{0.5}$	Remazol Red	Slurry ZnO	Yatmaz et al. [29]	2004	Separately, k_a correlated to different parameters: $[W]$, $[C]_0$ and I_0 .
5	$0.12 I_0^{1.79}$	$0.42 I_0^{0.37}$	$\frac{0.05 I_0^{2.16}}{1 + 0.12 I_0^{1.79} [C]_0}$	Acid Yellow 23	Slurry ZnO	Behnajady et al. [27]	2006	K and k_r obtained as a function of I_0 . Then, the experimental k_a values compared with the calculated values.
6	-	-	$0.005 [W]^{0.65} [C]_0^{-0.96} [O_2]^{0.16} I_0$	Acid Red 27	Slurry P25 TiO ₂	Behnajady & Modirshahla [30]	2006	Separately, k_a correlated to different parameters. Then, k_a correlated to the combined parameters.
7	-	$0.9243 I_0^{0.53}$	-	Diclofenac	Immobilized catalysts: P25 and modified TiO ₂	Hashim et al. [28]	2014	k_r correlated to different I_0 .
8	0.081	0.74	$\frac{k_r K}{1 + K [C]_0}$	Aid Orange 7	Immobilized P25 TiO ₂	Sheidaei & Behnajady [46]	2015	K and k_r values obtained by fitting k_a values to initial dye concentrations.
9	0.165	$9.86 [C]_0^{-0.69}$ $0.64 [W]_0^{0.73}$ $0.14 I_0^{0.91}$	$\frac{0.15 [C]_0^{-0.69} [W]_0^{0.73} I_0^{0.91}}{1 + 0.17 [C]_0}$	Direct Blue 15	Slurry P25 TiO ₂	This work	-	At optimized pH, K has a constant value. k_r obtained as a function of $[C]_0$, $[W]$, and I_0 . The experimental k_a values compared with the calculated values.
10	-	-	$0.77 [C]_0^{-1.65} [W]_0^{0.73} I_0^{0.89}$	Direct Blue 15	Slurry P25 TiO ₂	This work	-	Power law empirical model

3.4. Immobilized Catalyst

3.4.1. Surface Characterization

Figure 14 shows the thin film's surface microstructure at (A) low and (B) high magnifications. It is observed that the TiO_2 nanoparticles were deposited on the glass substrate with relatively non-uniform distribution. The thin film microstructure mainly consists of agglomerated spheres that accumulate on each other, resulting in spherical particles' multilayers, as shown in Figure 14A. In Figure 14B, the magnified image indicates that the texture was a rough surface with an irregular shape, resulting in surface heterogeneity. It is also obvious that the film microstructure refers to the presence of many voids of different sizes and shapes. These characteristics lead to obtaining a highly porous structure with different surface roughness. However, the presence of such surface properties is advantageous in terms of enhancing surface adsorption properties. The organic pollutants can easily attach to sharp and irregular edges compared to a smooth surface. Besides, the presence of such sharp and irregular edges increases the surface area available for molecules adsorption. Moreover, the light would easily penetrate the structure's surface pores, resulting in absorb large amounts of light and subsequently more degradation.

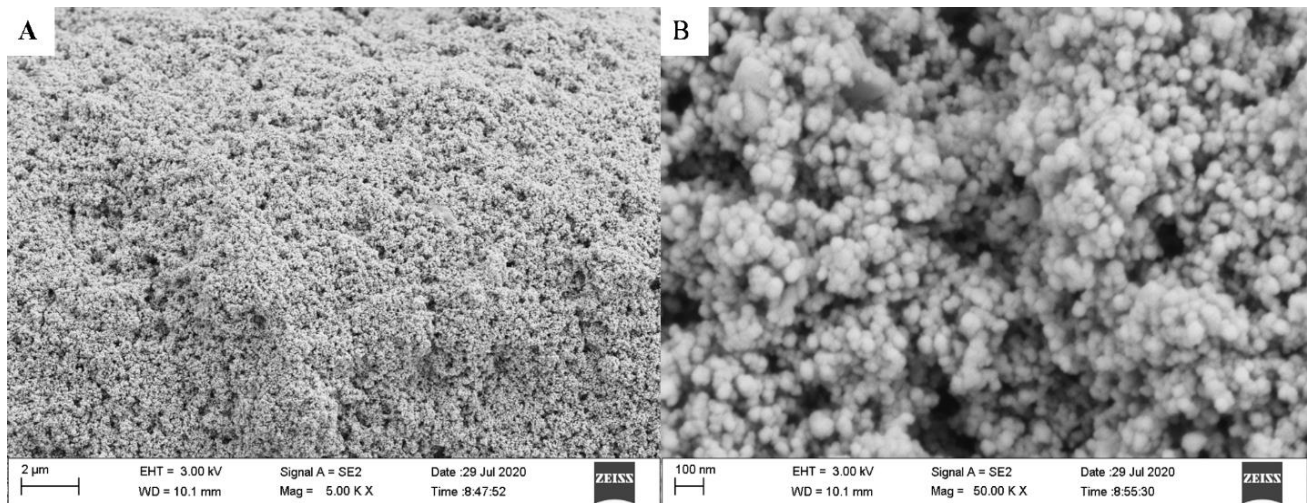


Figure 14. SEM images (A) low and (B) high magnifications of TiO_2 thin film coated on the Pyrex glass substrate.

Figure 15 shows the SEM micrograph of the surface morphology of TiO_2 thin film. It was noticed that the surface morphology mainly consists of a single or chain of like-cluster structures without a specific size that is uniformly distributed on the surface substrate. The captured image shows that the distribution of like-cluster structures leads to empty areas among them without particle aggregation. Such variance in areas appears a visible difference between the height of the like-cluster structures and actual film thickness. The inset in Figure 15 displays a high magnification of a selected area, which presents both single and chains of like-cluster structures that are formed due to TiO_2 particles agglomeration. Based on different chosen areas, the height of like-cluster structures was also determined. The SEM images showed that the height of like-cluster structures ranged between 132 to 140 μm , as shown in Figure 16.

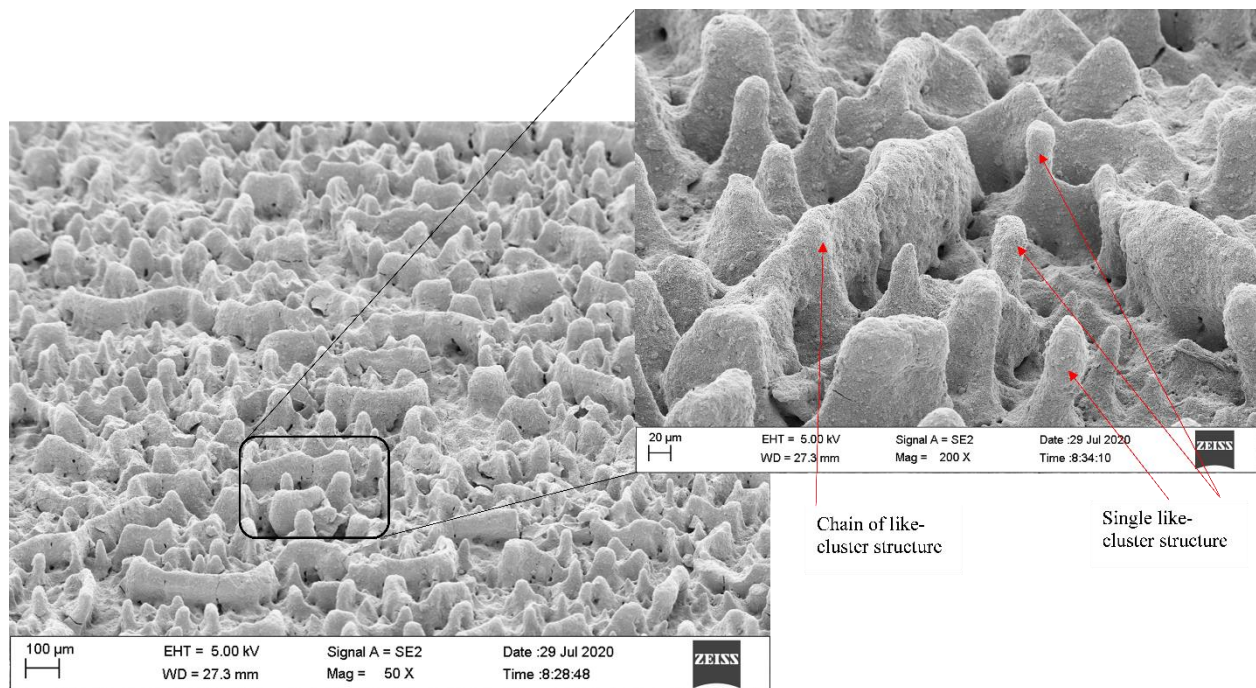


Figure 15. SEM micrographs of TiO₂ surface morphology coated on the Pyrex glass substrate.

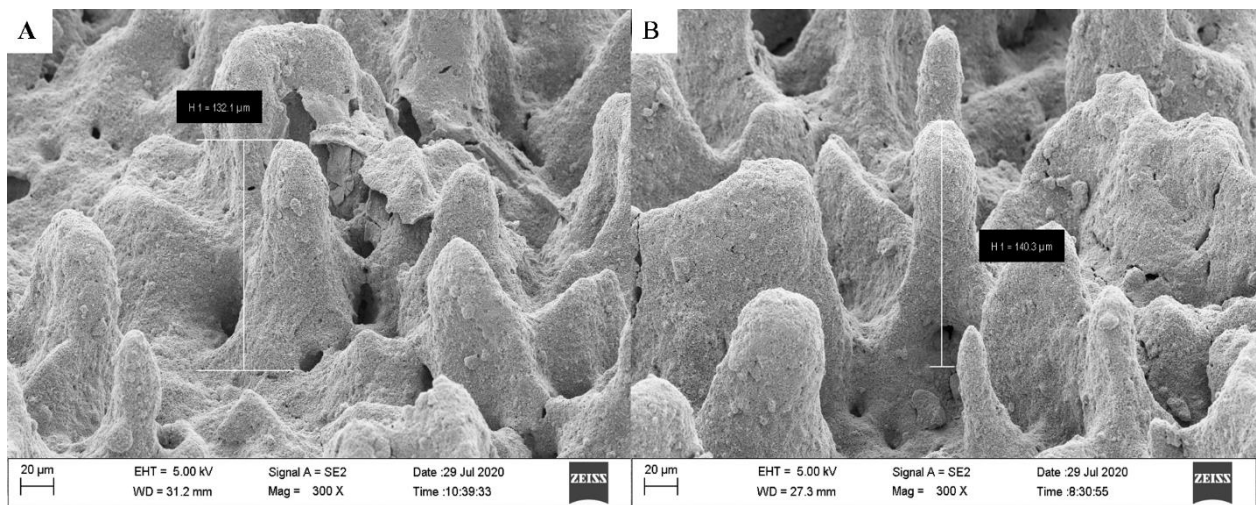


Figure 16. SEM micrographs of TiO₂'s like-cluster structures with a height of (A) 132 (B) 140 µm distributed on its surface.

3.4.2. Kinetics Using a Fixed Catalyst

The obtained results of DB15 degradation kinetics at different conditions for catalyst immobilization are shown in Table 8 and Figure 17. Table 8 demonstrates that linear fit was acquired for different initial concentrations. This refers to the pseudo first-order model that can describe the degradation kinetics of DB15 dye. For a catalyst density of $8.72 \times 10^4 \text{ Kg/m}^2$, it is observed the k_a value increases as the initial concentration is decreased. The k_a value increases from 5.65 to 35.11×10^{-3} when the initial concentration is decreased from 25 to 9 mg/L. It is noteworthy that a significant variance was registered for k_a values between slurry and immobilized catalyst. Such variation could be attributed to many factors. The main reason is that there is a clear difference in the experiments' pH values. While the slurry catalyst experiments were performed at the optimized pH value (pH 4), the immobilized catalyst experiments were conducted at natural pH (about 5.5). As discussed earlier in the pH optimization section, this pH difference significantly impacts dye degradation. When the pH value decreases from 5.5 to 4, the dye degradation

is improved dramatically. This is mainly attributed to enhancing adsorption properties because of the attractive force between the dye (included four sulfonate groups) and the positively charged catalyst surface. Hence, the degradation would be further increased. Another reason is the internal and external mass transfer effect. There are no limitations and effects for mass transfer between the bulk solution and catalyst surface for slurry catalysts. In contrast, there are some limitations for external mass transfer between the bulk concentration and catalyst surface. In addition, the internal mass transfer has major effects on the overall reaction rates. These limitations mainly control some reactions, as widely reported in the relevant literature [32].

Table 8. Kinetics data obtained for catalyst P25 immobilization at different reaction conditions.

N	Dye Concentration mg/L	Catalyst Density Kg/m ² × 10 ⁴	Light Intensity (W/m ²)	pH	k _a × 10 ³ (min ⁻¹)
1	25	8.72	11.2		5.65
2	20	8.72	11.2		7.89
3	16	8.72	11.2		11.33
4	12	8.72	11.2		19.2
5	9	8.72	11.2	Natural pH	35.11
6	10	1.46	1		1.92
7	10	1.46	2.5		2.68
8	10	1.46	6.1		4.41
9	10	1.46	11.2		6.25

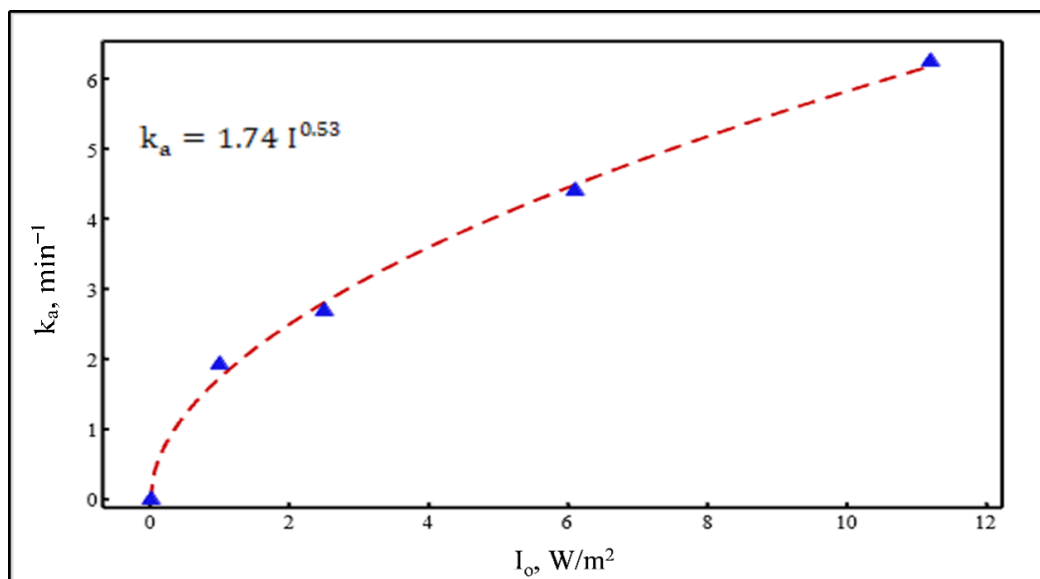


Figure 17. Non-linear regression of k_a values vs. different light intensities.

The effect of light intensity on k_a values for catalyst immobilization is presented in Figure 17. It is well known that light intensity plays a significant influence on the degradation reaction rate. The degradation rate constant typically has a power-law relation with light intensity. It has been reported that the degradation rate constant has a square root relation with the light intensity at the high range while the relation follows first order at the lower intensities range [26]. By plotting k_a values vs. their corresponding light intensities, the light intensity-dependent equation was obtained. With the use of non-linear regression, the best fit equation of the experimental values was then determined. Based on the MINITAB 19 software package (Version 19.2020.1) (Minitab, LLC, State College, PA, USA) analysis, the obtained equation was:

$$k_a = 1.74 I_0^{0.53} \quad (21)$$

It is concluded that the obtained equation is consistent with the relevant literature. Yatmaz et al. [29] found that k_a constant correlates to the square root of the light intensity through the degradation of RR dye over ZnO. As discussed earlier, the values of a and b for the slurry catalyst were 0.14 and 0.91, respectively. Chen and Ray [45] found a value of 0.84 for the photocatalytic degradation of 4-nitrophenol.

3.4.3. Catalyst Recyclability

The reusability test is considered of great importance for immobilized photocatalysts. Thus, a group of experiments were carried out at the same operating conditions to evaluate the extent of catalyst reusability. The recyclability was examined for up to four cycles, and the findings are displayed in Figure 18. As can be seen, there was no significant change, only 2.6%, in the catalyst activity after the second cycle. Compared to the original activity, the third cycle shows the catalyst activity reduced by 5.6%. After the fourth cycle, it appears that the catalyst lost 9.71% of its activity, registering a higher loss of activity. In this cycle, the DB15 degradation removal was reduced to 82.33% from 91.18% for the first use. The obtained results indicated that the immobilized catalyst possesses high reusability. However, the loss of catalyst activity could be explained by two reasons. The catalyst loses some of its particles over the cycles, and the catalyst washing after cycles. The second reason is catalyst surface contamination. Some dye molecules could be accumulated over the cycles that could compete with the following experiments' molecules for the limited active sites of the catalyst surface, resulting in a reduction in catalyst activity [47].

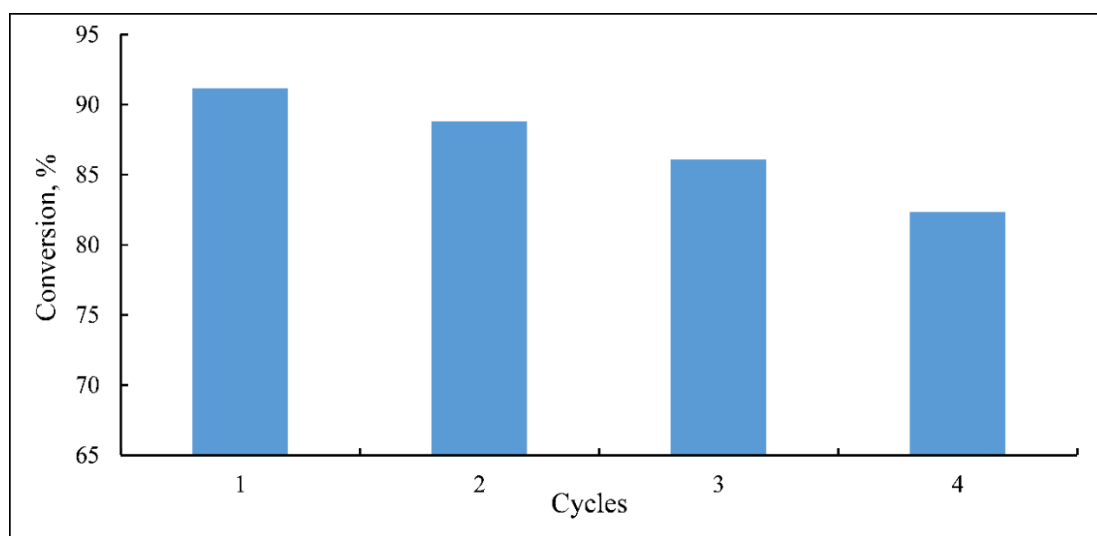


Figure 18. Recyclability of thin film TiO₂ catalyst at the conditions (natural pH, catalyst density $8.72 \times 10^{-4} \text{ Kg m}^{-2}$, light intensity 9.7 W/m^2 and dye concentration 13 mg/L).

3.5. DB15 Mineralization

The DB15 mineralization at 40 mg/L was discussed from the perspective of TOC removal, and their outcomes are shown in Figure 19 and Table 9. Figure 19 reveals the UV-Vis spectra of DB15 decolorization at natural pH and a dye concentration of 40 mg/L. It is observed that 82.5% dye decolorization was achieved within a reaction time of 4 hrs, while a complete color removal was obtained within 7 h. Although decolorization was achieved within a few hours, this did not mean the dye was completely mineralized. Decolorization refers to the color removal of a dye solution due to a bond cleavage responsible for the color of a dye; mineralization typically indicates conversion of carbon molecule within a dye structure to CO₂. For dye decolorization experiments, the volume of the treated dye solution was 250 mL using a catalyst concentration of 1 g/L. To reduce the time of DB15 mineralization, some parameters were changed while the dye concentration was kept constant at 40 mg/L. To achieve this, the catalyst concentration was increased to

2 g/L while the treated volume was lowered to 200 mL. Table 9 shows the obtained results of DB15 mineralization. As can be seen, the amount of remaining carbon was 4.02 mg, registering 75.55% carbon removal after a reaction time of 14 h. Meanwhile, the percentage of carbon removal increases to reach 83.64% when the reaction time is extended to 16 h. It is noteworthy that the time of complete mineralization would be longer than 16 h, although DB15 decolorization was achieved within a few hours. It should be noted that the model dye used in this study has a molecular weight of 992.8 g/mol, and hence would generate many reaction intermediates. The generated by-products properties could be different from the parental compound. Thus, the mineralization time would be dependent on the number and nature of the intermediates. To confirm the outcomes, the experiment of reaction time (16 h) was repeated. As shown in Table 9, the percentage of carbon removal was almost the same, indicating to results' reliability and reproducibility".

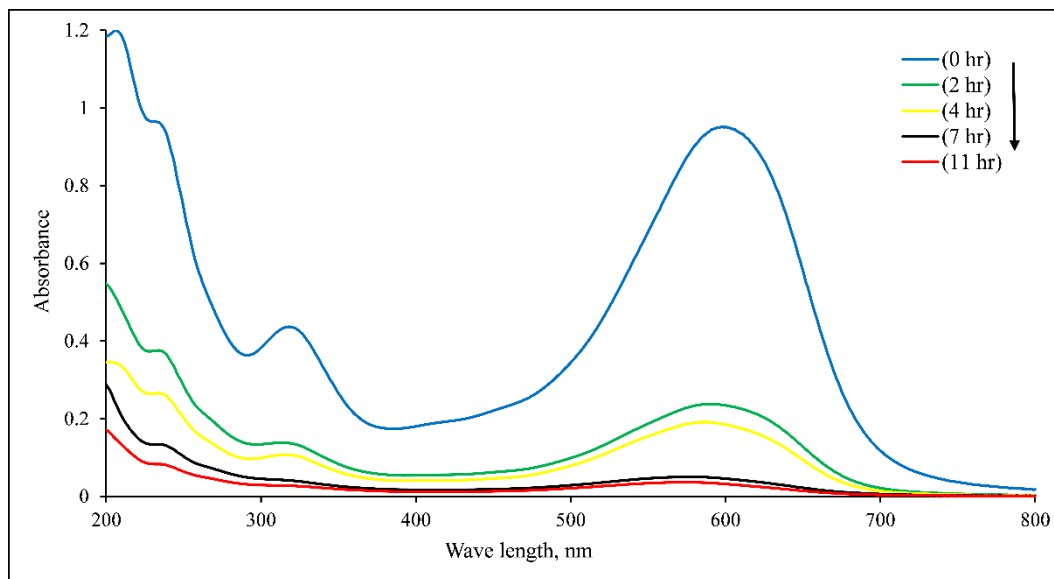


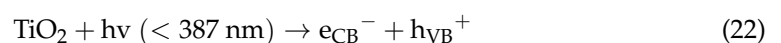
Figure 19. UV-Vis spectra of DB15 decolorization at 40 mg/L, catalyst 1 g/L, natural pH, and light intensity 11.2 W/m².

Table 9. DB15 mineralization at dye concentration 40 mg/L, natural pH, catalyst 2 g/L, light intensity 11.2 W/m², and treated volume 200 mL.

N	Amount of Original Carbon, mg/L	Amount of Remaining Carbon, mg/L	Carbon Removal, %	Reaction Time, h
1	16.44	4.020	75.55	14
2	16.44	2.690	83.64	16
3	16.44	2.677	83.72	16

3.6. Mechanism of DB15 Degradation at Low pH

The absorbed photons with energies equal to or higher than the energy bandgap (E_g) of the P25 photocatalyst initiate an excitation for the valence band (VB) electrons. Then, the excited electrons will be instantaneously promoted from the VB to the conduction band (CB), resulting in the generation of electron-hole pairs [48–53]. Simultaneously, as the pH value of experiments was 4, which is lower than the pzc of P25, the TiO₂ surface is positively charged as shown below:



The pH has a significant effect on the possible reaction mechanisms of dye degradation; namely, direct dye oxidation with a positive hole, direct dye reduction with an electron

in the CB, and hydroxyl radical (OH^\bullet) attack [15,17,25]. In terms of the OH^\bullet attack mechanism, it is known that the OH^\bullet radicals are generated via the reactions between positive holes and adsorbed water and hydroxide ions (OH^-) [49,50,53,54] as in the following equations:



As the pH solution was low (pH 4), the reaction of positive holes and adsorbed water seems to be more dominant due to the low availability of OH^- (acidic medium). However, the generated OH^\bullet radicals have less impact than positive holes on dye degradation at these conditions. It was considered that positive holes represent the main contributor of oxidation among different species at lower pH values while OH^\bullet radicals are dominant oxidizers at higher pH values [15,24].

Meanwhile, the photogenerated electrons can react with the adsorbed O_2 molecules on the catalyst surface or dissolved O_2 in water to produce a superoxide radical anion ($\text{O}_2^{\bullet-}$) [49,50,53–58]. The generated $\text{O}_2^{\bullet-}$ can be protonated by the highly available H^+ ions (pH 4) and by the previously generated H^+ via the reaction of h_{VB}^+ with the adsorbed H_2O molecules. This leads to forming hydroperoxyl radicals (HO_2^\bullet) [50,53,55,57,58] as shown below:



With respect to direct dye reduction, pH is considered a significant factor because of its major role in the reductive cleavage of azo bonds at low pH values [15]. As part of the direct dye oxidation mechanism, the generated positive holes directly react with the DB15 to produce intermediate compounds that mineralize to CO_2 and H_2O eventually as final products of the oxidation process, as presented in Equation (28). The general mechanism of DB15 degradation at a low pH value is displayed in Figure 20 [28].

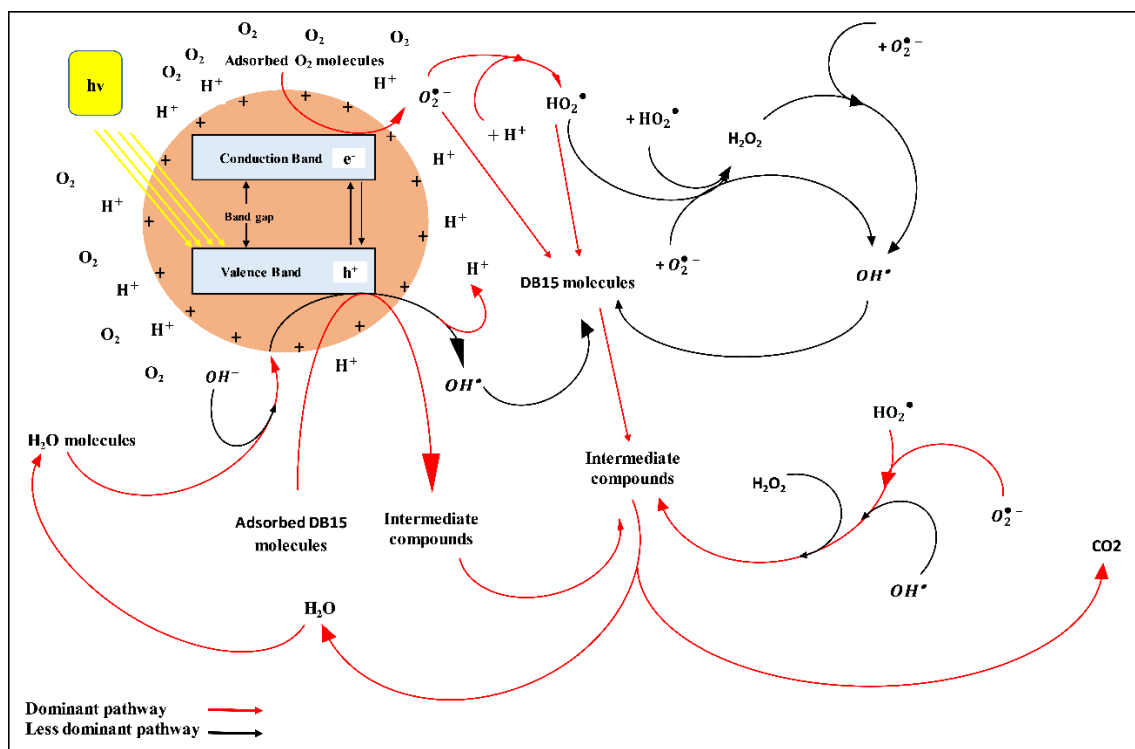


Figure 20. General mechanism of DB15 degradation at low pH value.

3.7. Adsorption Behaviour of DB15

The influence of pH on the photodegradation process needs to be analyzed to understand adsorption behavior, especially since it was constant for all experiments. The analysis of pH impact on dye photodegradation is a highly complex task due to its multiple functions. It has a major effect on the ionization state of a catalyst surface, reactants, and products [15,16]. The surface charge of the catalyst surface is directly related to pH. The catalyst surface can be protonated and deprotonated under acidic and alkaline conditions, respectively. Therefore, pH significantly impacts the adsorption of dyes onto the catalyst surface and thus governs the entire photodegradation process [4,15,24,26,45].

As shown earlier, the value of K is 0.165 L mg^{-1} . It was previously reported that dye photodegradation increases when the pH value is lowered [59,60]. Strong adsorption was observed at low pH values ($\text{pH} < \text{pzc}$) for dye molecules on the TiO_2 surface due to the attractive force between the positively charged TiO_2 surface and the dye molecules. For a similar reason, many studies concluded that the maximum photodegradation of different dyes over the Degussa P25 catalyst is within acidic conditions. Such dye types include Metanil Yellow, Acid Orange 7, Acid Black 1, Acid Red 14, and Reactive Black 5 [4,17,48,61]. This behavior could be explained because those were anionic dyes that included at least one anionic group (sulfonate group) in their chemical structure. Strong adsorption occurs on the catalyst surface due to the attraction force between the surface's positive charge and the sulfonate groups. Such adsorption becomes more favorable at low pH values ($\text{pH} < \text{pzc}$). Thus, the photodegradation rate enhances as the pH value is lowered. Sleiman et al. [4] observed that Metanil Yellow's adsorption, which includes one sulfonate group, has a twofold increase compared to its value at neutral pH.

Based on the above, the strong adsorption between DB15 (four sulfonate groups) and the P25 surface due to the acidic medium (pH 4) is mainly responsible for the K value. In addition, as the pH value was constant for all experiments, obtaining a stable K value is quite reasonable. This is because of the major role of pH on the adsorption-desorption equilibrium and both catalyst surface and dye adsorption properties.

4. Conclusions

In this study, the degradation kinetics of DB15 over suspended and immobilized TiO_2 photocatalyst were examined. The degradation experiments were carried out in a swirl flow reactor under UV light irradiation for different catalyst modes. For the slurry catalyst, a group of experiments were performed to examine the optimum pH value for DB15 degradation at two different dye concentrations. The impact of three various factors: dye concentration, catalyst loading, and light intensity on the DB15 kinetics was discussed. The results of DB15 kinetics were analyzed using different pathways, namely, k_a approach, a single value of k_r and K , and approach of k_r as of variable. The DB15 mineralization was also investigated. In terms of immobilized catalyst, P25 was coated on a Pyrex glass using a dip-coating device. The coated thin film surface was characterized using an SEM test. Using an immobilized catalyst, the influence of initial dye concentration and light intensity on the DB15 degradation kinetics were examined. The thin film catalyst reusability was also evaluated. With respect to the k_a approach, the L-H model well describes the findings of this study. A pseudo first-order kinetics model registered for the influence of dye concentration on the DB15 kinetics. The catalyst loading and light intensity exhibited similar behavior to dye concentration on the degradation kinetics. L-H constant k_r was evaluated as a function of three variables. Then, the k_a values were determined and compared with their laboratory data. In terms of three variables, the developed model of k_a had the following form: $k_a = \frac{0.15 [C]_0^{-0.69} [W]^{0.73} I^{0.91}}{1+0.17 [C]_0}$ while the empirical model was $k_a = 0.77 [C]_0^{-1.65} [W]^{0.73} I^{0.89}$. The results showed that DB15 mineralization at 40 mg/L reaches up to 83.64% after a reaction time of 16 hrs. For immobilized catalysts, the pseudo first-order model fits well the DB15 kinetics for different dye concentrations, while a power-law model describes the influence of light intensity on the degradation kinetics.

The findings also revealed that the thin film was recyclable for up to four cycles with high durability.

Author Contributions: Conceptualization, A.K.R., A.P. and W.J.; methodology, A.K.R., A.P. and W.J.; software, A.K.R., A.P. and W.J.; validation, A.K.R., A.P. and W.J.; formal analysis, A.K.R., A.P., W.J.; investigation, W.J.; resources, A.P.; data curation, A.K.R.; writing—original draft preparation, W.J.; writing—review and editing, A.K.R. and A.P.; visualization, W.J.; supervision, A.K.R. and A.P.; project administration, A.P.; funding acquisition, A.K.R. and A.P. All authors have read and agreed to the published version of the manuscript.

Funding: This research received no external funding.

Institutional Review Board Statement: Not applicable.

Informed Consent Statement: Not applicable.

Acknowledgments: The authors are grateful to Todd Simpson in Western Nanofabrication Facility for doing an SEM test of the thin film of coated P25 on Pyrex glass. Many thanks are extended to Western University Machine Shop for the modification of the dip-coating device. The authors would like to thank Jonas Hedberg in Western Surface Science for testing few samples using a spectrophotometer to obtain a full scan range regarding DB15 decolorization.

Conflicts of Interest: The authors declare that there is no conflict of interest.

References

1. Cardoso, J.C.; Bessegato, G.G.; Zanoni, M.V.B. Efficiency comparison of ozonation, photolysis, photocatalysis and photoelectrocatalysis methods in real textile wastewater decolorization. *Water Res.* **2016**, *98*, 39–46. [[CrossRef](#)] [[PubMed](#)]
2. Karamat, N.; Ehsan, M.F.; Ashiq, M.N.; Ijaz, S.; Najam-ul-Haq, M.; Hamid, S.; Bahnemann, D.W. Synthesis, characterization and photocatalytic activity of LaNdZr₂O₇ supported SnSe nanocomposites for the degradation of Foron blue dye. *Appl. Surf. Sci.* **2019**, *463*, 1019–1027. [[CrossRef](#)]
3. Gong, R.; Ding, Y.; Li, M.; Yang, C.; Liu, H.; Sun, Y. Utilization of powdered peanut hull as biosorbent for removal of anionic dyes from aqueous solution. *Dye. Pigment.* **2005**, *64*, 187–192. [[CrossRef](#)]
4. Sleiman, M.; Vildoza, D.; Ferronato, C.; Chovelon, J.M. Photocatalytic degradation of azo dye Metanil Yellow: Optimization and kinetic modeling using a chemometric approach. *Appl. Catal. B Environ.* **2007**, *77*, 1–11. [[CrossRef](#)]
5. Nguyen, C.H.; Fu, C.C.; Juang, R.S. Degradation of methylene blue and methyl orange by palladium-doped TiO₂ photocatalysis for water reuse: Efficiency and degradation pathways. *J. Clean. Prod.* **2018**, *202*, 413–427. [[CrossRef](#)]
6. Hsiao, Y.C.; Wu, T.F.; Wang, Y.S.; Hu, C.C.; Huang, C. Evaluating the sensitizing effect on the photocatalytic decoloration of dyes using anatase-TiO₂. *Appl. Catal. B Environ.* **2014**, *148*, 250–257. [[CrossRef](#)]
7. Bouberka, Z.; Benabbou, K.A.; Khenifi, A.; Maschke, U. Degradation by irradiation of an Acid Orange 7 on colloidal TiO₂/(LDHs). *J. Photochem. Photobiol. A Chem.* **2014**, *275*, 21–29. [[CrossRef](#)]
8. Rosa, J.M.; Garcia, V.S.; Boiani, N.F.; Melo, C.G.; Pereira, M.C.; Borrelly, S.I. Toxicity and environmental impacts approached in the dyeing of polyamide, polyester and cotton knits. *J. Environ. Chem. Eng.* **2019**, *7*, 102973. [[CrossRef](#)]
9. Ajmal, A.; Majeed, I.; Malik, R.N.; Idriss, H.; Nadeem, M.A. Principles and mechanisms of photocatalytic dye degradation on TiO₂ based photocatalysts: A comparative overview. *RSC Adv.* **2014**, *4*, 37003–37026. [[CrossRef](#)]
10. Wang, C.C.; Li, J.R.; Lv, X.L.; Zhang, Y.Q.; Guo, G. Photocatalytic organic pollutants degradation in metal–organic frameworks. *Energy Environ. Sci.* **2014**, *7*, 2831–2867. [[CrossRef](#)]
11. Reutergårdh, L.B.; Iangphasuk, M. Photocatalytic decolorization of reactive azo dye: A comparison between TiO₂ and us photocatalysis. *Chemosphere* **1997**, *35*, 585–596. [[CrossRef](#)]
12. Galindo, C.; Jacques, P.; Kalt, A. Photodegradation of the aminoazobenzene acid orange 52 by three advanced oxidation processes: UV/H₂O₂, UV/TiO₂ and VIS/TiO₂: Comparative mechanistic and kinetic investigations. *J. Photochem. Photobiol. A Chem.* **2000**, *130*, 35–47. [[CrossRef](#)]
13. Houas, A.; Lachheb, H.; Ksibi, M.; Elaloui, E.; Guillard, C.; Herrmann, J.M. Photocatalytic degradation pathway of methylene blue in water. *Appl. Catal. B Environ.* **2001**, *31*, 145–157. [[CrossRef](#)]
14. Xu, Y.; Langford, C.H. UV-or visible-light-induced degradation of X3B on TiO₂ nanoparticles: The influence of adsorption. *Langmuir* **2001**, *17*, 897–902. [[CrossRef](#)]
15. Konstantinou, I.K.; Albanis, T.A. TiO₂-assisted photocatalytic degradation of azo dyes in aqueous solution: Kinetic and mechanistic investigations: A review. *Appl. Catal. B Environ.* **2004**, *49*, 1–14. [[CrossRef](#)]
16. Sauer, T.; Neto, G.C.; Jose, H.J.; Moreira, R.F.P.M. Kinetics of photocatalytic degradation of reactive dyes in a TiO₂ slurry reactor. *J. Photochem. Photobiol. A Chem.* **2002**, *149*, 147–154. [[CrossRef](#)]
17. Baran, W.; Adamek, E.; Makowski, A. The influence of selected parameters on the photocatalytic degradation of azo-dyes in the presence of TiO₂ aqueous suspension. *Chem. Eng. J.* **2008**, *145*, 242–248. [[CrossRef](#)]

18. Meng, Y.; Huang, X.; Wu, Y.; Wang, X.; Qian, Y. Kinetic study and modeling on photocatalytic degradation of para-chlorobenzoate at different light intensities. *Environ. Pollut.* **2002**, *117*, 307–313. [CrossRef]
19. Xu, Y.; Langford, C.H. Variation of Langmuir adsorption constant determined for TiO₂-photocatalyzed degradation of acetophenone under different light intensity. *J. Photochem. Photobiol. A Chem.* **2000**, *133*, 67–71. [CrossRef]
20. Konstantinou, I.K.; Albanis, T.A. Photocatalytic transformation of pesticides in aqueous titanium dioxide suspensions using artificial and solar light: Intermediates and degradation pathways. *Appl. Catal. B Environ.* **2003**, *42*, 319–335. [CrossRef]
21. Herrmann, J.M. Heterogeneous photocatalysis: Fundamentals and applications to the removal of various types of aqueous pollutants. *Catal. Today* **1999**, *53*, 115–129. [CrossRef]
22. Son, H.S.; Lee, S.J.; Cho, I.H.; Zoh, K.D. Kinetics and mechanism of TNT degradation in TiO₂ photocatalysis. *Chemosphere* **2004**, *57*, 309–317. [CrossRef] [PubMed]
23. Al-Ekabi, H.; Serpone, N. Photocatalytic degradation of chlorinated phenols in aerated aqueous solutions over TiO₂ supported on a glass matrix. *J. Phys. Chem.* **1988**, *92*, 5726–5731. [CrossRef]
24. Habibi, M.H.; Hassanzadeh, A.; Mahdavi, S. The effect of operational parameters on the photocatalytic degradation of three textile azo dyes in aqueous TiO₂ suspensions. *J. Photochem. Photobiol. A Chem.* **2005**, *172*, 89–96. [CrossRef]
25. Turchi, C.S.; Ollis, D.F. Photocatalytic degradation of organic water contaminants: Mechanisms involving hydroxyl radical attack. *J. Catal.* **1990**, *122*, 178–192. [CrossRef]
26. Zhou, S.; Ray, A.K. Kinetic studies for photocatalytic degradation of Eosin B on a thin film of titanium dioxide. *Ind. Eng. Chem. Res.* **2003**, *42*, 6020–6033. [CrossRef]
27. Behnajady, M.A.; Modirshahla, N.; Hamzavi, R. Kinetic study on photocatalytic degradation of CI Acid Yellow 23 by ZnO photocatalyst. *J. Hazard. Mater.* **2006**, *133*, 226–232. [CrossRef]
28. Hashim, N.; Natarajan, P.; Ray, A.K. Intrinsic kinetic study for photocatalytic degradation of diclofenac under UV and visible light. *Ind. Eng. Chem. Res.* **2014**, *53*, 18637–18646. [CrossRef]
29. Yatmaz, H.C.; Akyol, A.; Bayramoglu, M. Kinetics of the photocatalytic decolorization of an azo reactive dye in aqueous ZnO suspensions. *Ind. Eng. Chem. Res.* **2004**, *43*, 6035–6039. [CrossRef]
30. Behnajady, M.A.; Modirshahla, N. Nonlinear regression analysis of kinetics of the photocatalytic decolorization of an azo dye in aqueous TiO₂ slurry. *Photochem. Photobiol. Sci.* **2006**, *5*, 1078–1081. [CrossRef]
31. Ray, A.K.; Beenackers, A.A. Novel swirl-flow reactor for kinetic studies of semiconductor photocatalysis. *AIChE J.* **1997**, *43*, 2571–2578. [CrossRef]
32. Chen, D.; Li, F.; Ray, A.K. External and internal mass transfer effect on photocatalytic degradation. *Catal. Today* **2001**, *66*, 475–485. [CrossRef]
33. Zangeneh, H.; Zinatizadeh, A.A.L.; Feyzi, M. Degradation of linear alkyl benzene using an immobilized nano TiO₂ photocatalytic reactor: Process analysis and modeling. *CLEAN–Soil Air Water* **2016**, *44*, 78–88. [CrossRef]
34. Arabatzis, I.M.; Antonaraki, S.; Stergiopoulos, T.; Hiskia, A.; Papaconstantinou, E.; Bernard, M.C.; Falaras, P. Preparation, characterization and photocatalytic activity of nanocrystalline thin film TiO₂ catalysts towards 3, 5-dichlorophenol degradation. *J. Photochem. Photobiol. A Chem.* **2002**, *149*, 237–245. [CrossRef]
35. Javidi Soufiani, M. Investigation and Modeling of Dip-Coating Process for Dispersions. Ph.D. Thesis, The University of Western Ontario, London, ON, Canada, 2016; p. 75. Available online: <https://ir.lib.uwo.ca/etd/3641> (accessed on 13 September 2021).
36. Deng, Z.; Zhang, X.H.; Chan, K.C.; Liu, L.; Li, T. Fe-based metallic glass catalyst with nanoporous surface for azo dye degradation. *Chemosphere* **2017**, *174*, 76–81. [CrossRef]
37. Jadaa, W.; Prakash, A.; Ray, A.K. Modeling of degradation of Diazo dye in swirl-flow photocatalytic reactor: Response surface approach. *Catalysts* **2020**, *10*, 1418. [CrossRef]
38. Matthews, R.W. Kinetics of photocatalytic oxidation of organic solutes over titanium dioxide. *J. Catal.* **1988**, *111*, 264–272. [CrossRef]
39. Mills, A.; Morris, S. Photomineralization of 4-chlorophenol sensitized by titanium dioxide: A study of the initial kinetics of carbon dioxide photogeneration. *J. Photochem. Photobiol. A Chem.* **1993**, *71*, 75–83. [CrossRef]
40. Hamad, H.A.; Sadik, W.A.; El-Latif, M.A.; Kashyout, A.B.; Feteha, M.Y. Photocatalytic parameters and kinetic study for degradation of dichlorophenol-indophenol (DCPIP) dye using highly active mesoporous TiO₂ nanoparticles. *J. Environ. Sci.* **2016**, *43*, 26–39. [CrossRef]
41. Boumaza, S.; Kaouah, F.; Hamane, D.; Trari, M.; Omeiri, S.; Bendjama, Z. Visible light assisted decolorization of azo dyes: Direct Red 16 and Direct Blue 71 in aqueous solution on the p-CuFeO₂/n-ZnO system. *J. Mol. Catal. A Chem.* **2014**, *393*, 156–165. [CrossRef]
42. Chan, Y.C.; Chen, J.N.; Lu, M.C. Intermediate inhibition in the heterogeneous UV-catalysis using a TiO₂ suspension system. *Chemosphere* **2001**, *45*, 29–35. [CrossRef]
43. Sadik, W.A. Decolourization of an azo dye by heterogeneous photocatalysis. *Process Saf. Environ. Prot.* **2007**, *85*, 515–520. [CrossRef]
44. Augugliaro, V.; Palmisano, L.; Schiavello, M.; Sclafani, A.; Marchese, L.; Martra, G.; Miano, F. Photocatalytic degradation of nitrophenols in aqueous titanium dioxide dispersion. *Appl. Catal.* **1991**, *69*, 323–340. [CrossRef]
45. Chen, D.; Ray, A.K. Photodegradation kinetics of 4-nitrophenol in TiO₂ suspension. *Water Res.* **1998**, *32*, 3223–3234. [CrossRef]

46. Sheidaei, B.; Behnajady, M.A. Mathematical kinetic modelling and representing design equation for a packed photoreactor with immobilised TiO₂-P25 nanoparticles on glass beads in the removal of CI Acid Orange 7. *Chem. Process Eng.* **2015**, *36*, 125–133. [[CrossRef](#)]
47. Teixeira, S.; Martins, P.M.; Lanceros-Méndez, S.; Kühn, K.; Cuniberti, G. Reusability of photocatalytic TiO₂ and ZnO nanoparticles immobilized in poly (vinylidene difluoride)-co-trifluoroethylene. *Appl. Surf. Sci.* **2016**, *384*, 497–504. [[CrossRef](#)]
48. Daneshvar, N.; Salari, D.; Khataee, A.R. Photocatalytic degradation of azo dye acid red 14 in water: Investigation of the effect of operational parameters. *J. Photochem. Photobiol. A Chem.* **2003**, *157*, 111–116. [[CrossRef](#)]
49. Ahmed, S.; Rasul, M.G.; Brown, R.; Hashib, M.A. Influence of parameters on the heterogeneous photocatalytic degradation of pesticides and phenolic contaminants in wastewater: A short review. *J. Environ. Manag.* **2011**, *92*, 311–330. [[CrossRef](#)] [[PubMed](#)]
50. Teh, C.M.; Mohamed, A.R. Roles of titanium dioxide and ion-doped titanium dioxide on photocatalytic degradation of organic pollutants (phenolic compounds and dyes) in aqueous solutions: A review. *J. Alloys Compd.* **2011**, *509*, 1648–1660. [[CrossRef](#)]
51. Daneshvar, N.; Salari, D.; Niaei, A.; Rasoulifard, M.H.; Khataee, A.R. Immobilization of TiO₂ nanopowder on glass beads for the photocatalytic decolorization of an azo dye CI Direct Red 23. *J. Environ. Sci. Health Part A* **2005**, *40*, 1605–1617. [[CrossRef](#)]
52. Carp, O.; Huisman, C.L.; Reller, A. Photoinduced reactivity of titanium dioxide. *Prog. Solid State Chem.* **2004**, *32*, 33–177. [[CrossRef](#)]
53. Akpan, U.G.; Hameed, B.H. Parameters affecting the photocatalytic degradation of dyes using TiO₂-based photocatalysts: A review. *J. Hazard. Mater.* **2009**, *170*, 520–529. [[CrossRef](#)]
54. Khataee, A.R.; Kasiri, M.B. Photocatalytic degradation of organic dyes in the presence of nanostructured titanium dioxide: Influence of the chemical structure of dyes. *J. Mol. Catal. A Chem.* **2010**, *328*, 8–26. [[CrossRef](#)]
55. Umar, M.; Aziz, H.A. Photocatalytic degradation of organic pollutants in water. In *Organic Pollutants-Monitoring, Risk and Treatment*; InTech: Rijeka, Croatia, 2013.
56. Zhang, T.; Wang, X.; Zhang, X. Recent progress in TiO₂-mediated solar photocatalysis for industrial wastewater treatment. *Int. J. Photoenergy* **2014**, *2014*, 607954. [[CrossRef](#)]
57. Zangeneh, H.; Zinatizadeh, A.A.L.; Habibi, M.; Akia, M.; Isa, M.H. Photocatalytic oxidation of organic dyes and pollutants in wastewater using different modified titanium dioxides: A comparative review. *J. Ind. Eng. Chem.* **2015**, *26*, 1–36. [[CrossRef](#)]
58. Khaki, M.R.D.; Shafeeyan, M.S.; Raman, A.A.A.; Daud, W.M.A.W. Application of doped photocatalysts for organic pollutant degradation—A review. *J. Environ. Manag.* **2017**, *198*, 78–94. [[CrossRef](#)]
59. Bandara, J.; Mielczarski, J.A.; Kiwi, J. 2. Photosensitized degradation of azo dyes on Fe, Ti, and Al oxides. Mechanism of charge transfer during the degradation. *Langmuir* **1999**, *15*, 7680–7687. [[CrossRef](#)]
60. Sakthivel, S.; Neppolian, B.; Shankar, M.V.; Arabindoo, B.; Palanichamy, M.; Murugesan, V. Solar photocatalytic degradation of azo dye: Comparison of photocatalytic efficiency of ZnO and TiO₂. *Sol. Energy Mater. Sol. Cells* **2003**, *77*, 65–82. [[CrossRef](#)]
61. Poullos, I.; Tsachpinis, I. Photodegradation of the textile dye Reactive Black 5 in the presence of semiconducting oxides. *J. Chem. Technol. Biotechnol. Int. Res. Process Environ. Clean Technol.* **1999**, *74*, 349–357. [[CrossRef](#)]